ADVANCED OPTICAL MATERIALS

Supporting Information

for *Adv. Optical Mater.*, DOI: 10.1002/adom.202001994

Blue Emissive *fac*/*mer*-Iridium (III) NHC Carbene Complexes and their Application in OLEDs

Muazzam Idris, Savannah C. Kapper, Abegail C. Tadle, Thilini Batagoda, Daniel Sylvinson Muthiah Ravinson, Opeoluwa Abimbola, Peter I. Djurovich, Jongchan Kim, Caleb Coburn, Stephen R. Forrest, and Mark E. Thompson**

Supporting Information

Blue Emissive *fac*/*mer*-Iridium (III) NHC Carbene Complexes and their Application in OLEDs

Muazzam Idris,[a,⊕] Savannah C. Kapper,[a,⊕] Abegail C. Tadle,[a] Thilini Batagoda,[a] Daniel Sylvinson Muthiah Ravinson,[a] Opeoluwa Abimbola, [b] Peter Djurovich,[a] Jongchan Kim,[c] Caleb Coburn,[c] Stephen R. Forrest[*,c,d,e] and Mark E. Thompson[*,a]

[a] Department of Chemistry, University of Southern California, Los Angeles, California 90089, USA.
[b] Department of Chemical Engineering, University of Southern California, Los Angeles, California 90089, USA.
[c] Department of Physics, University of Michigan, Ann Arbor, Michigan 48109, USA.
[d] Department of Electrical and Computer Engineering, University of Michigan, Ann Arbor, Michigan 48109, USA.
[e] Department of Materials Science and Engineering, University of Michigan, Ann Arbor, Michigan 48109, USA.

⊕: These two authors contributed equally to this work.
* : Author to whom correspondence should be addressed, met@usc.edu.

General Information

Reactions were carried out under nitrogen unless otherwise noted. NMRs were obtained using a Varian 400 MHz NMR. Absorbance and molar absorptivity measurements were taken using a Hewlett-Packard 4853 diode array spectrophotometer. A Hamamatsu integrating sphere was used to obtain quantum yields of all solutions. Lifetime measurements were obtained using a Time-Correlated Single Photon Counting (TCSPC). Steady state excitation and emission spectra were obtained at both room temperature and 77 K through use of a Photon Technology International QuantaMaster model C-60SE spectrofluorimeter. 2-Methyltetrahydrofuran was used as the solvent unless otherwise stated. Both Cyclic Voltammetry (CV) and Differential pulse voltammetry (DPV) were performed through use of an EG&G potentiostat/galvanostat model 283. The electrolyte was composesd of 0.1 M tetra-n-butylammonium hexafluorophosphate in acetonitrile. The measurements were taken under an inert atmosphere. The working, counter, and pseudoreference electrodes were composed of glassy carbon, platinum wire, and silver wire respectively. The ferrocene redox couple was used as the internal references for all electrochemistry measurements. For thermal degredation studies, thin films were prepared by spin coating on quartz substrates from dichloromethane solutions. The thin films were thermally degraded at 100 ^{o}C under nitrogen. Photoluminescence data of the fresh and aged samples were taken from their respective thin films. High resolution mass spectra were recorded using a Bruker Autoflex Speed MALDI-TOF spectrometer. Samples for mass spectroscopy were prepared by dissolving the films in dichloromethane and depositing the solution on a MALDI plate.

Synthesis

Synthesis of N2-phenylpyrazine-2,3-diamine (2)

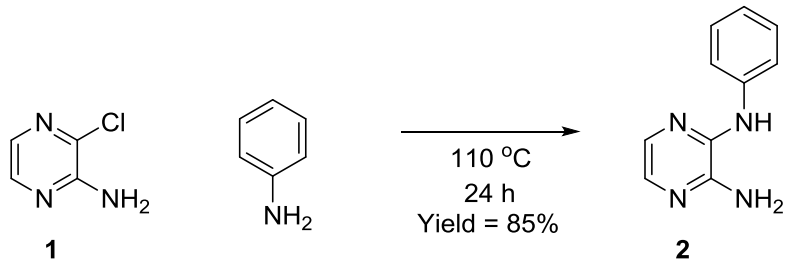

1 **2**

To a one-necked 500-mL round bottom flask, 3-chloropyrazin-2-amine (10.00 g, 77.19 mmol) and aniline (7.19 g, 77.19 mmol) were added and heated for 24 hours at 100 °C. After cooling to room temperature, the reaction mixture was dissolved in water and brought to a pH of 7 using a 25% solution of sodium bicarbonate. The product was extracted using dichloromethane (CH_2Cl_2). The resulting organic phases were further dissolved in CH_2Cl_2 by vigorous stirring overnight. The resulting solution was dried over sodium sulfate and concentrated to dryness. The residue was washed with diethyl ether resulting in a brownish yellow powder. Yield: 12.22 g, 85%. Spectra match those reported in the literature.[1]

Synthesis of 1-phenyl-1H-imidazo[4,5-b]pyrazine (3)

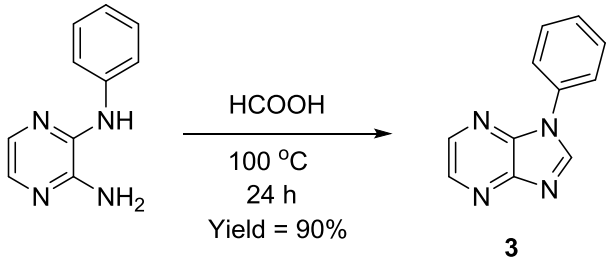

3

A solution of N2-phenylpyrazine-2,3-diamine (10.00 g, 53.70 mmol) in formic acid (324 mL, 8.60 mol) was refluxed for 24 hours. The reaction mixture was evaporated to dryness and the residue was dissolved in CH_2Cl_2 and extracted with saturated sodium bicarbonate solution. The organic phase was dried with sodium sulfate and evaporated to dryness. Yield: 9.49 g, 90%. ^{1}H NMR (400 MHz, $CDCl_3$) δ 8.63 (s, 1H), 8.61 (d, *J* = 2.6 Hz, 1H), 8.41 (d, *J* = 2.6 Hz, 1H), 7.76

– 7.71 (d, 2H), 7.58 (t, 1H), 7.47 (t, 1H). ^{13}C NMR (101 MHz, $CDCl_3$) δ 149.38, 145.77, 140.70, 139.71, 139.23, 134.44, 130.02, 128.46, 123.20.

Synthesis of 1-methyl-3-phenyl-1H-imidazo[4,5-b]pyrazin-1-ium iodide (4)

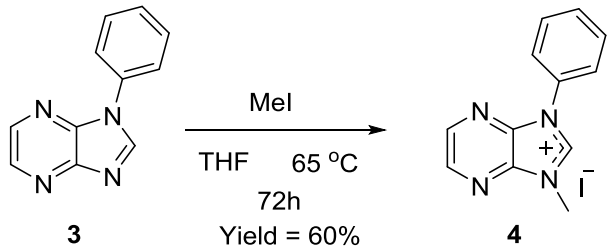

In a 500ml pressure flask, 1-phenyl-1H-imidazo[4,5-b]pyrazine (8.00 g, 40.77 mmol) and methyl iodide (5.79 g, 40.77 mmol) were dissolved in 100 mL THF and stirred at 60 °C for 72 hours. Afterwards the reaction mixture was cooled down to room temperature and the precipitate was filtered, washed with diethyl ether and dried under vacuo. According to ^{1}H-NMR and ^{13}C-NMR, methylation occurred on the imidazole nitrogen and one of the pyrazino nitrogens. These products were not separated and were carried to the next step without further purification. Yield = 8.34 g, 60%. ^{1}H NMR (400 MHz, DMSO-d_6) δ 10.74 (s, J = 0.7 Hz, 1H), 9.86 (s, 1H), 9.16 – 9.11 (m, 2H), 9.02 (d, J = 2.6 Hz, 1H), 8.97 (d, J = 2.6 Hz, 1H), 7.94 – 7.88 (m, 4H), 7.79 – 7.59 (m, 6H), 4.60 – 4.48 (s, 3H), 4.17 (s, J = 0.6 Hz, 3H). ^{13}C NMR (101 MHz, DMSO-d_6) δ 154.08, 146.68, 146.12, 144.04, 144.03, 141.32, 138.02, 137.57, 133.36, 132.81, 132.51, 130.97, 130.58, 130.45, 130.05, 125.15, 124.60, 42.11, 32.79.

Synthesis of mer-tris-(N-phenyl,N-methyl-pyrizinoimidazol-2-yl)iridium (III) (*mer*-Ir(pmpz)$_3$)

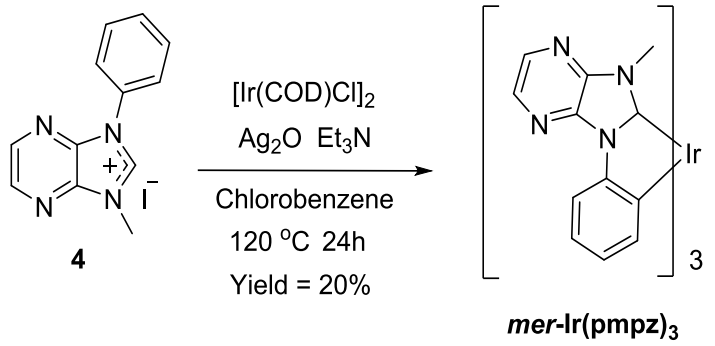

To a 250 ml round bottomed one necked flask, 1-methyl-3-phenyl-1H-imidazo[4,5-b]pyrazin-1-ium iodide (9.06 g, 26.8 mmol), bis(1,5-cyclooctadiene)diiridium(I) dichloride (3.00 g, 4.47 mmol) and silver (I) oxide (0.621 g, 2.68 mmol) were added. The reaction flask was purged with nitrogen and evacuate three times. 100 mL of degassed chlorobenzene and triethylamine (0.271 g, 2.68 mmol) were added to the flask. The reaction mixture was stirred in the dark at 120 °C for 24 hours. After the reaction was complete, chlorobenzene was removed under reduced pressure and the residue was purified by column chromatography on silica using hexane and ethyl acetate (6:4) as the eluent. Yield = 736 mg, 20%. ^{1}H NMR (400 MHz, $CDCl_3$) δ 8.71 (ddd, *J* = 7.9, 1.3, 0.5 Hz, 1H), 8.67 (ddd, *J* = 7.9, 1.3, 0.5 Hz, 1H), 8.61 (ddd, *J* = 7.9, 1.3, 0.5 Hz, 1H), 8.37 (d, *J* = 2.8, 2H), 8.32 (d, *J* = 2.9 Hz, 1H), 8.29 (d, *J* = 2.9 Hz, 2H), 8.23 (d, *J* = 2.9 Hz, 1H), 7.12 – 7.01 (m, 3H), 6.95 – 6.89 (m, 2H), 6.82 (td, *J* = 7.3, 1.2 Hz, 1H), 6.75 (m, 2H), 6.57 (dd, *J* = 7.3, 1.2, 1H), 3.39 (s, 3H), 3.37 (s, 3H), 3.27 (s, 3H). ^{13}C NMR (101 MHz, $CDCl_3$) δ 193.87, 190.47, 189.65, 148.00, 147.24, 146.90, 145.68, 145.50, 143.20, 142.07, 142.00, 141.85, 139.82, 139.79, 139.75, 139.04, 138.52, 137.61, 137.32, 136.69, 136.64, 136.05, 135.68, 126.14, 126.03, 125.82, 122.10, 121.61, 121.48, 115.18, 115.03, 114.56, 32.19, 32.11, 31.22. Elemental Analysis: Anal. Calcd. for $C_{36}H_{27}IrN_{12}$: C, 52.7; H, 3.32; N, 20.5. Found: C, 52.1; H, 3.34; N 19.7.

Synthesis of fac-tris-(N-phenyl,N-methyl-pyrizinoimidazol-2-yl)iridium (III) (*fac*-Ir(pmpz)$_3$)

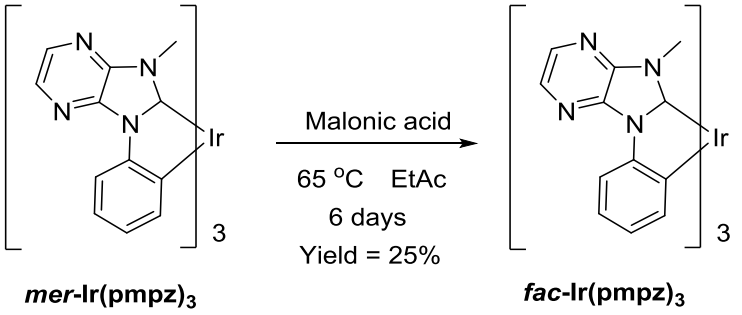

mer-tris-(N-phenyl,N-methyl-pyrizinoimidazol-2-yl)iridium (III) (0.10 g, 0.121 mmol) was added to a 100 mL pressure tube under nitrogen atmosphere. Degassed ethyl acetate (12 mL) and 2 mL of 1M aqueous solution of malonic acid were added to the tube. The tube was sealed and stirred for 6 days at 65 °C. The reaction was extracted with CH_2Cl_2 and purified on silica with hexanes/ethyl acetate mixture (50/50). Yield = 25 mg, 25%. ^{1}H NMR (400 MHz, $CDCl_3$) δ 8.67 (dd, *J* = 7.9, 0.8 Hz, 1H), 8.33 (d, *J* = 2.9 Hz, 1H), 8.22 (d, *J* = 2.9 Hz, 1H), 7.13 (td, *J* = 7.9, 7.3, 1.5 Hz, 1H), 6.81 (td, *J* = 7.3, 1.3 Hz, 1H), 6.57 (dd, *J* = 8.8, 1.7 Hz, 1H), 3.41 (s, 3H). ^{13}C NMR (101 MHz, $CDCl_3$) δ 194.83, 146.73, 144.56, 141.85, 139.85, 137.43, 136.37, 136.25, 126.05, 122.25, 114.66, 32.14. Elemental Analysis: Anal. Calcd. for $C_{36}H_{27}IrN_{12}$: C, 52.7; H, 3.3; N, 20.5. Found: C, 51.2; H, 3.85; N 18.0.

Synthesis of N2,N3-di-p-tolylpyrazine-2,3-diamine (5)

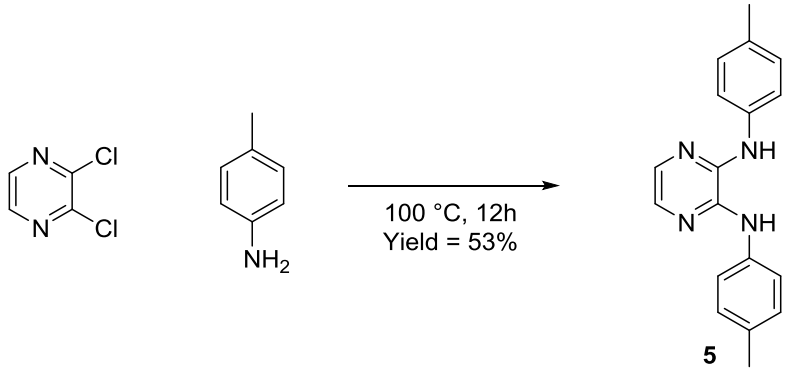

To a 100-mL round bottom flask, 2,3-dichloropyrazine (10.00 g, 67.13 mmol) and p-toluidine (15.82 g, 147.68 mmol) were added and heated overnight at 100 °C. After cooling to room temperature, the reaction mixture was dissolved in water and brought to a pH of 7 using a 25% solution of sodium hydroxide. The product was extracted using dichloromethane. The resulting organic phases were dried over sodium sulfate and concentrated to dryness. The residue was washed with petroleum ether resulting in an off-white powder. Yield: 10.124 g, 53%. ^{1}H NMR (400 MHz, DMSO-d_6) δ 9.83 – 9.49 (b, 2H), 7.60 (d, J = 8.4 Hz, 4H), 7.41 (s, 2H), 7.16 (d, J = 8.4 Hz, 4H), 2.27 (s, 6H). ^{13}C NMR (101 MHz, DMSO-d_6) δ 141.31, 137.02, 132.75, 129.69, 127.04, 121.63, 20.96.

Synthesis of 2-ethoxy-1,3-di-p-tolyl-2,3-dihydro-1H-imidazo[4,5-b]pyrazine (6)

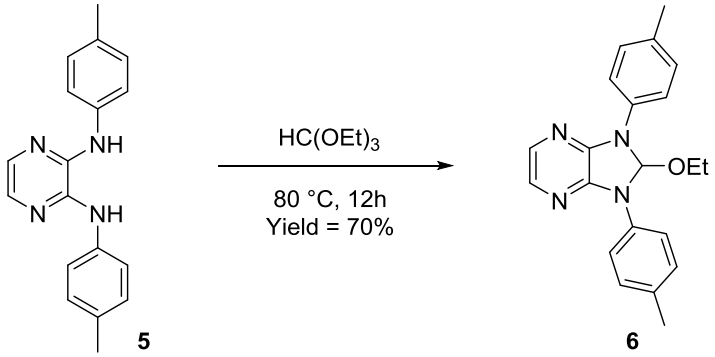

The 2,3-bis(N-phenylamino)pyrazine (4.00 g, 13.8 mmol) was placed in a flask with $HC(OEt)_3$ (70 mL, 0.415 mol) that acted as both the solvent and reactant. The reaction was stirred overnight at 80 °C. In the morning, the reaction was cooled to room temperature and the mixture was filtered. A large amount of white powder was left in the filter. The solvent from the filtrate was removed under reduced pressure and the product was recrystallized in petroleum ether. The product was allowed to dry over the weekend to ensure it was dry enough for the next step. Yield: 3.33 g, 70%. ^{1}H NMR (400 MHz, $CDCl_3$) δ 7.87 (d, *J* = 2.1 Hz, 4H), 7.49 (s, 2H), 7.24 (d, *J* = 2.1 Hz, 4H), 7.19 (s, 1H), 3.33 (q, *J* = 7.0 Hz, 2H), 2.36 (s, 6H), 1.07 (t, *J* = 7.0 Hz, 3H). ^{13}C NMR (101 MHz, $CDCl_3$) δ 143.63, 135.36, 133.86, 130.37, 129.75, 118.90, 96.29, 55.17, 20.89, 14.51.

Synthesis of fac-tris-(N-tolyl,N-tolyl-pyrizinoimidazol-2-yl)iridium (III) (*fac*-Ir(tpz)$_3$)

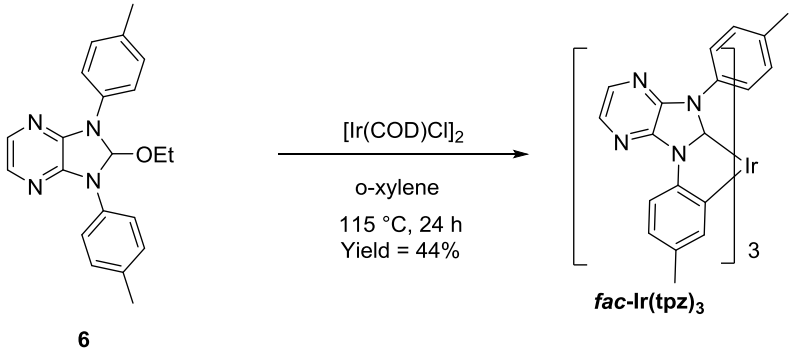

To a 150-mL round bottom flask, molecular sieves (3 Å, 5 g), bis(1,5-cyclooctadiene)diiridium(I) dichloride (0.60 g, 0.89 mmol), and 2-ethoxy-1,3-di-p-tolyl-2,3-dihydro-1H-imidazo[4,5-b]pyrazine (3.09 g, 8.93 mmol) were added to the flask. The flask was pumped and purged three times. O-xylene (120 mL) purged with nitrogen gas was added to the reaction flask and heated to 115 °C for 24 hours. The product was purified on silica using hexane and dichloromethane (80:20). The product was obtained and recrystallized in dichloromethane. Yield: 0.43 g, 44%. ^{1}H NMR (400 MHz, $CDCl_3$) δ 8.60 (d, *J* = 8.0 Hz, 1H), 8.30 (d, *J* = 2.9 Hz, 1H), 8.02 (d, *J* = 2.9 Hz, 1H), 6.96 (ddd, *J* = 8.0, 2.0, 0.8 Hz, 1H), 6.56 – 6.50 (m, 1H), 2.13 (s, 3H), 1.88 (s, 3H), 1.55 (d, *J* = 40.0 Hz, 3H). ^{13}C NMR (101 MHz, $CDCl_3$) δ 194.57, 145.41, 144.19, 143.04, 139.76, 138.96, 137.01, 135.96, 135.16, 132.94, 128.63, 122.79, 114.55, 21.63, 20.94. Elemental Analysis: Anal. Calcd. for $C_{57}H_{45}IrN_{12}$: C, 62.8; H, 4.16; N, 15.4. Found: C, 62.6; H, 4.17; N 15.0.

Electrochemical and Photophysical Properties

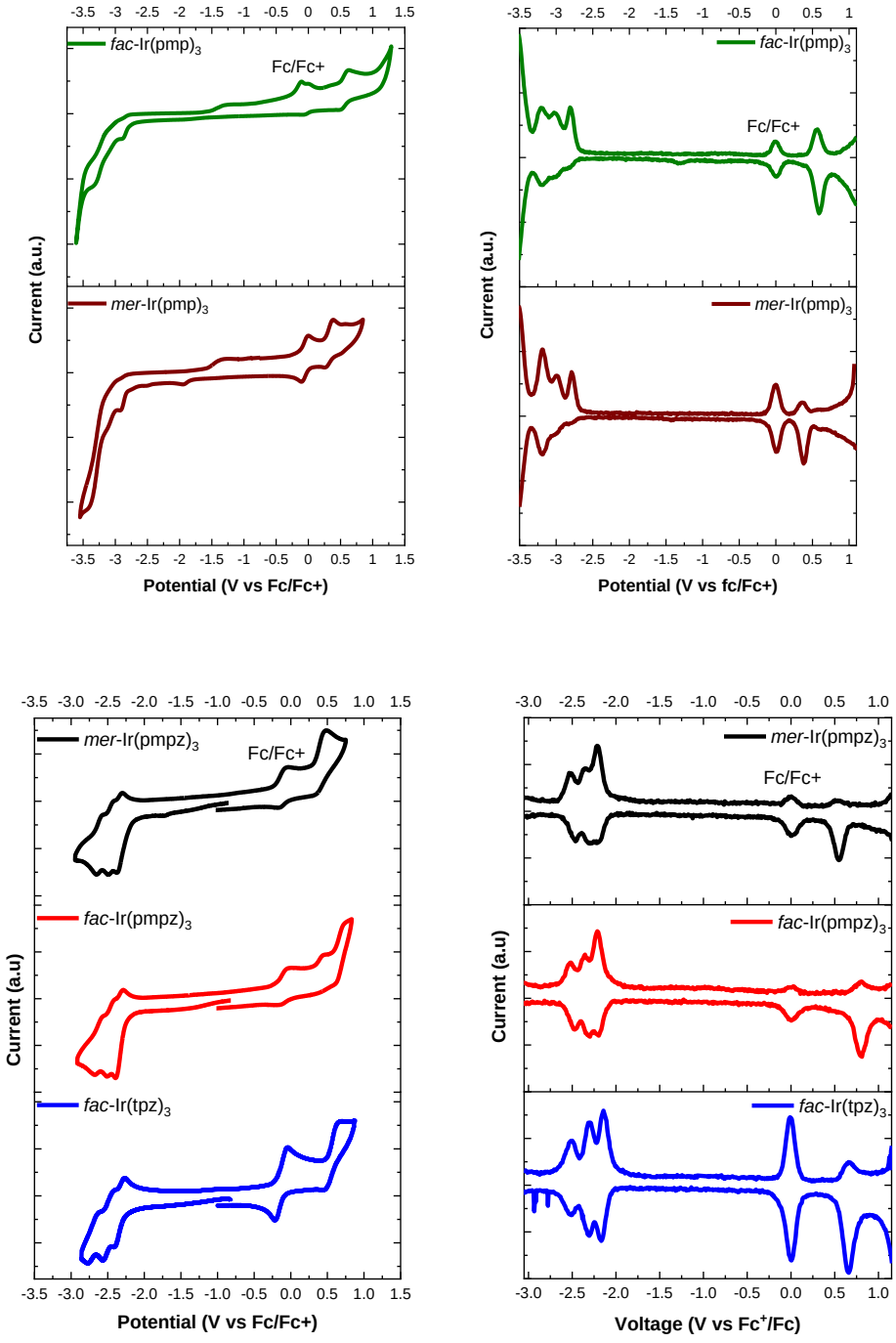

Figure S1. Voltammetry data of Ir(C^C:)$_3$ complexes.

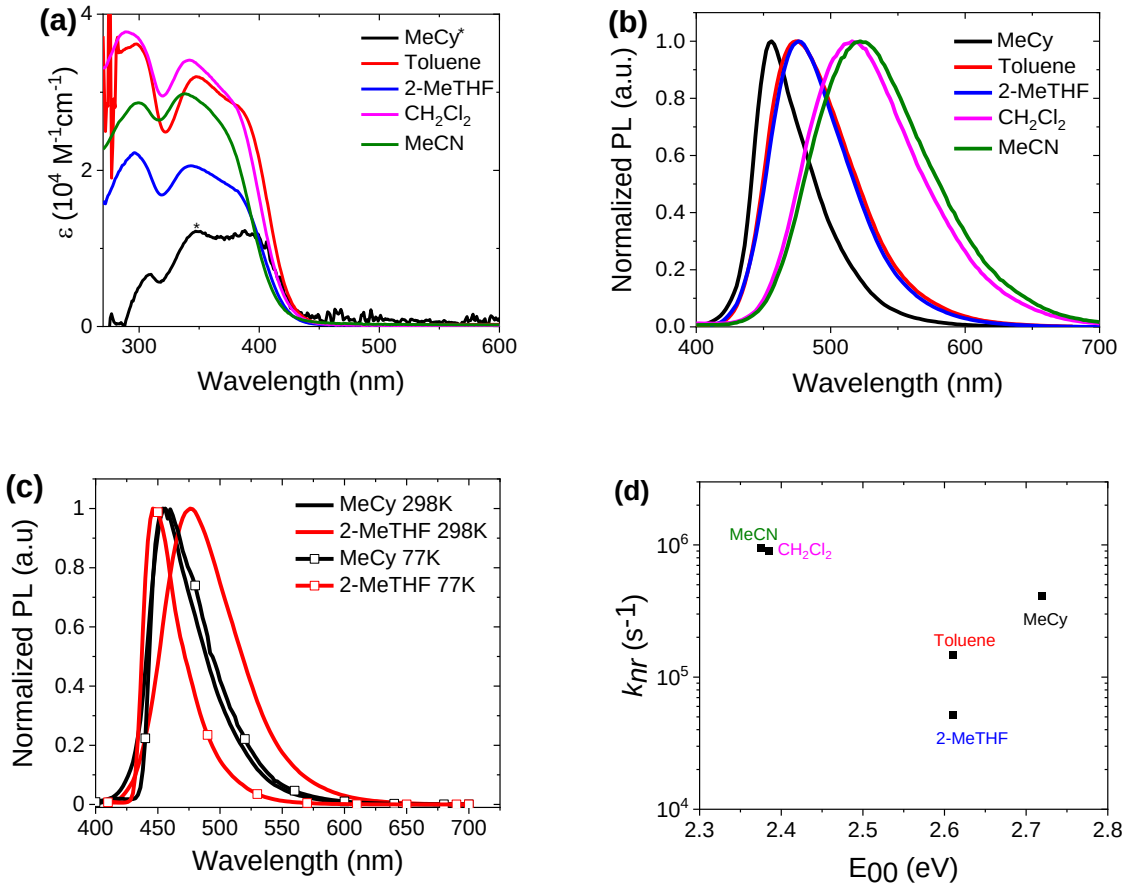

Figure S2. Photophysical properties of *fac*-Ir(pmpz)$_3$. (a) UV-visible spectra in various solvents at 298K (**fac*-Ir(pmpz)$_3$ is highly insoluble in MeCy), (b) PL spectra in various solvents at 298K, (c) PL spectra in MeCy and 2-MeTHF at 298K and 77K (d) Energy gap law plot at room temperature.

Table S1. Photophysical properties of *fac*-Ir(pmpz)$_3$ in various solvents at 298K and 77K.

Solvent (298K)	λ_{max} (nm)	τ (μs)	Φ	k_r (s^{-1}) x10^5	k_{nr} (s^{-1}) x10^5
MeCy	456	1.55	0.67	4.32	4.13
Toluene	474	1.85	0.73	3.95	1.46
2-MeTHF	476	2.5	0.87	3.48	0.52
CH_2Cl_2	516	0.793	0.29	3.66	8.95
MeCN	522	0.763	0.27	3.54	9.57
MeCy 77K	454	5.54	---	---	---
2-MeTHF 77K	446	7.5	---	---	---

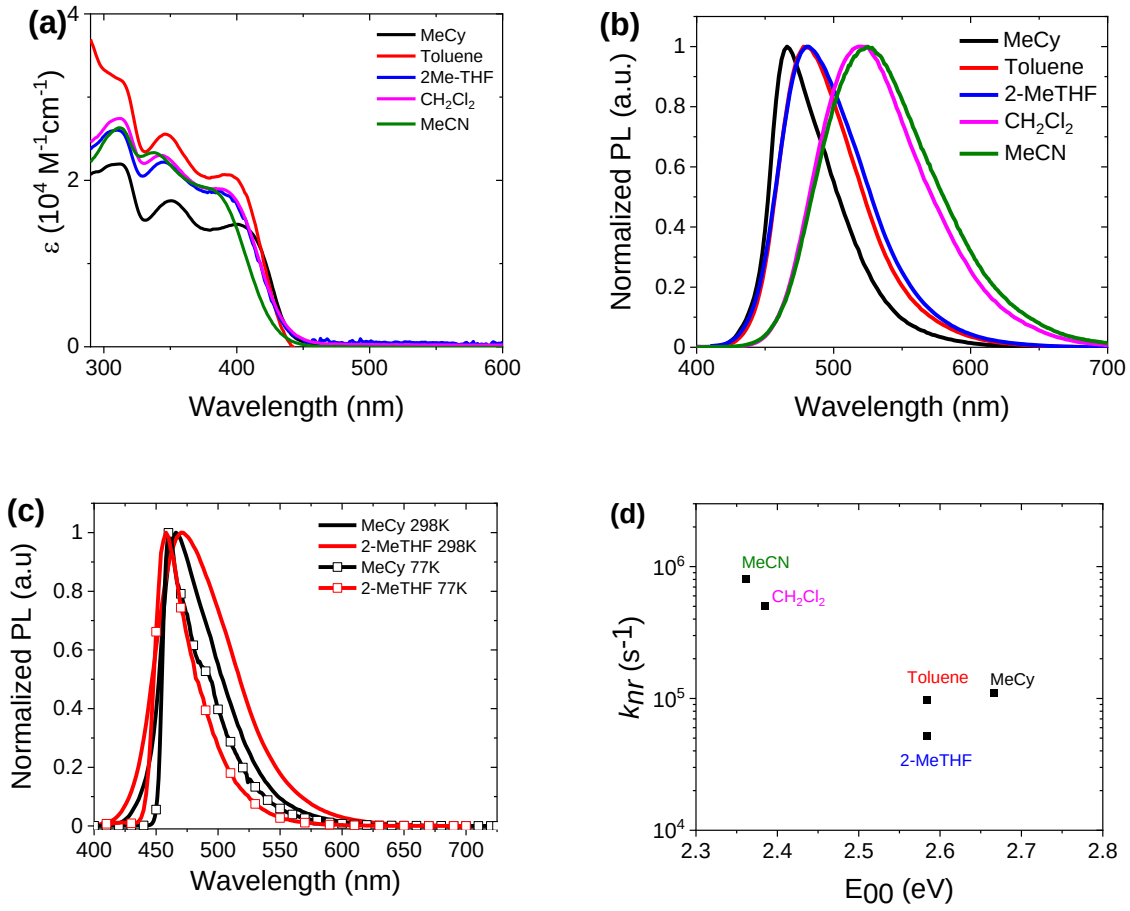

Figure S3. Photophysical properties of *fac*-Ir(tpz)$_3$. (a) UV-visible spectra in various solvents at 298K, (b) PL spectra in various solvents at 298K, (c) PL spectra in MeCy and 2-MeTHF at 298K and 77K (d) Energy gap law plot at room temperature.

Table S2. Photophysical properties of *fac*-Ir(tpz)$_3$ in various solvents at 298K and 77K.

Solvent (298K)	λ_{max} (nm)	τ (μs)	Φ	k_r (s^{-1}) x10^5	k_{nr} (s^{-1}) x10^5
MeCy	466	2.2	0.76	3.5	1.1
Toluene	478	2.1	0.89	4.2	0.52
2-MeTHF	470	2.0	0.98	4.9	0.98
CH_2Cl_2	520	1.1	0.45	4.1	5.0
MeCN	525	0.86	0.31	3.6	8.0
MeCy 77K	461	4.0	---	---	---
2-MeTHF 77K	458	4.4	---	---	---

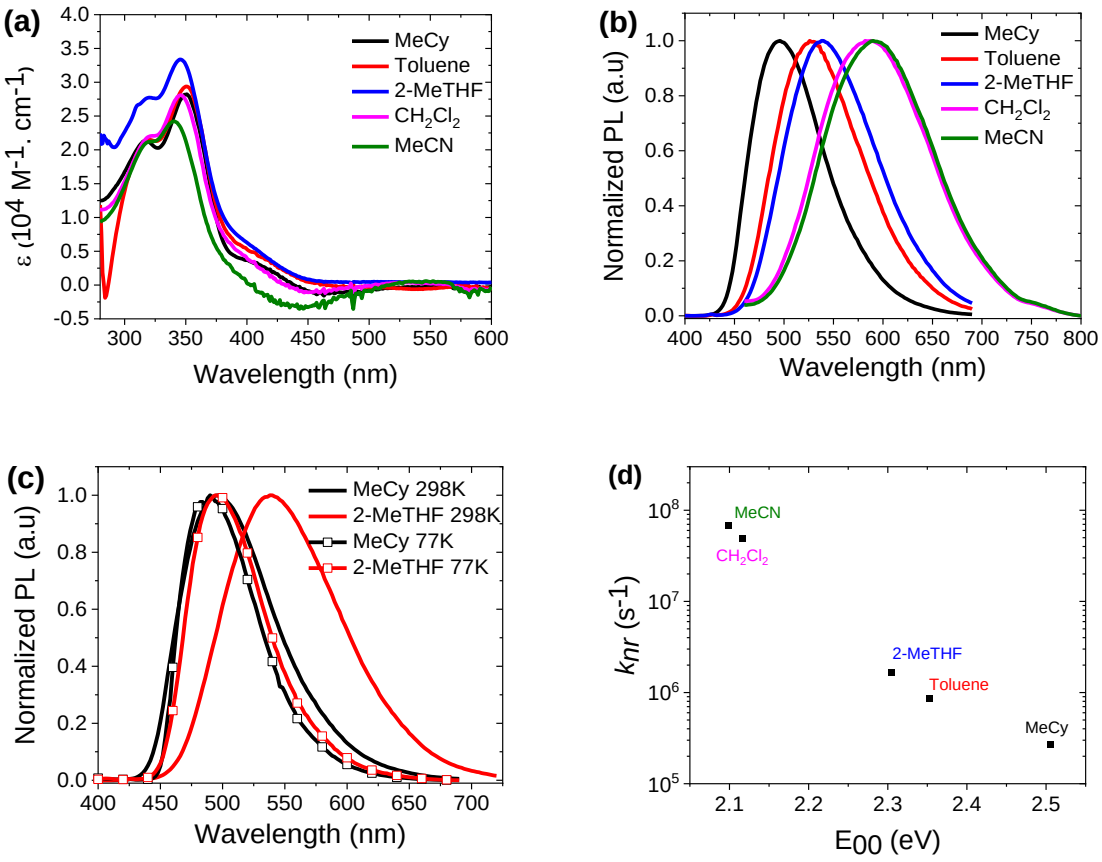

Figure S4. Photophysical properties of *mer*-Ir(pmpz)$_3$. (a) UV-visible spectra in various solvents at 298K, (b) PL spectra in various solvents at 298K, (c) PL spectra in MeCy and 2-MeTHF at 298K and 77K, (d) Energy gap law plot at room temperature.

Table S3. Photophysical properties of *mer*-Ir(pmpz)$_3$ in various solvents at 298K and 77K.

Solvent (298K)	λ_{max} (nm)	τ (μs)	Φ	k_r (s^{-1}) x10^5	k_{nr} (s^{-1}) x10^5
MeCy	496	0.89	0.76	8.50	2.68
Toluene	526	0.60	0.49	8.19	8.53
2-MeTHF	538	0.44	0.27	6.21	16.8
CH_2Cl_2	588	0.02	0.012	6.03	496
MeCN	590	0.015	0.008	5.44	675
MeCy 77K	490	1.61	---	---	---
2-MeTHF 77K	494	2.00	---	---	---

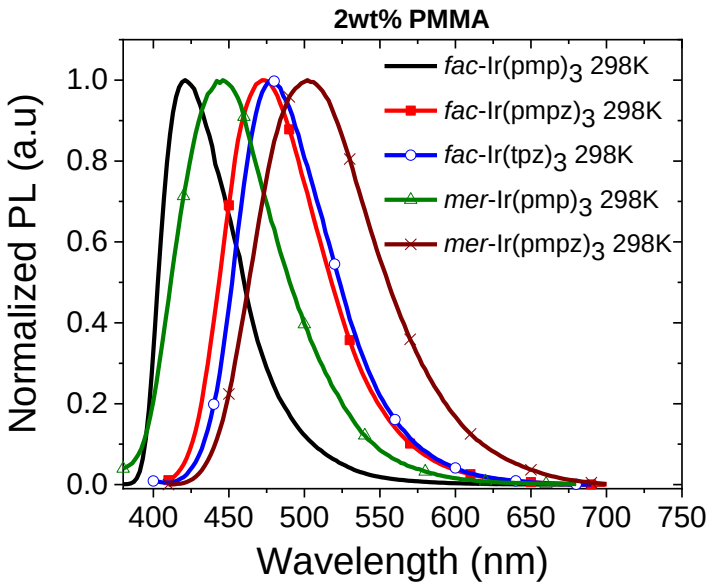

Figure S5. Emission spectra of Ir-carbene complexes in PMMA.

Table S4. Photophysical properties of Ir-carbene complexes in PMMA (2 wt%) at 298K.

complex	λ_{max} (nm)	Φ_{PL}	τ (μs)	k_r (s^{-1}) x10^5	k_{nr} (s^{-1}) x10^5
fac-Ir(pmp)$_3$	420	0.54	1.34	4.0	3.4
fac-Ir(pmpz)$_3$	470	0.82	1.80	4.6	1.0
fac-Ir(tpz)$_3$	478	0.92	1.91	4.8	0.42
mer-Ir(pmp)$_3$	445	0.66	0.70	9.4	4.8
mer-Ir(pmpz)$_3$	500	0.74	0.47	16	5.5

Thermal Degradation Studies

The goal of the experiment is to study the thermal degradation of different phosphors in order to compare their chemical stabilities. The experiment explored ligand loss of FIrpic, $Ir(ppy)_3$ and $Ir(tpz)_3$ under thermal conditions with Bphen as a chemical trap.

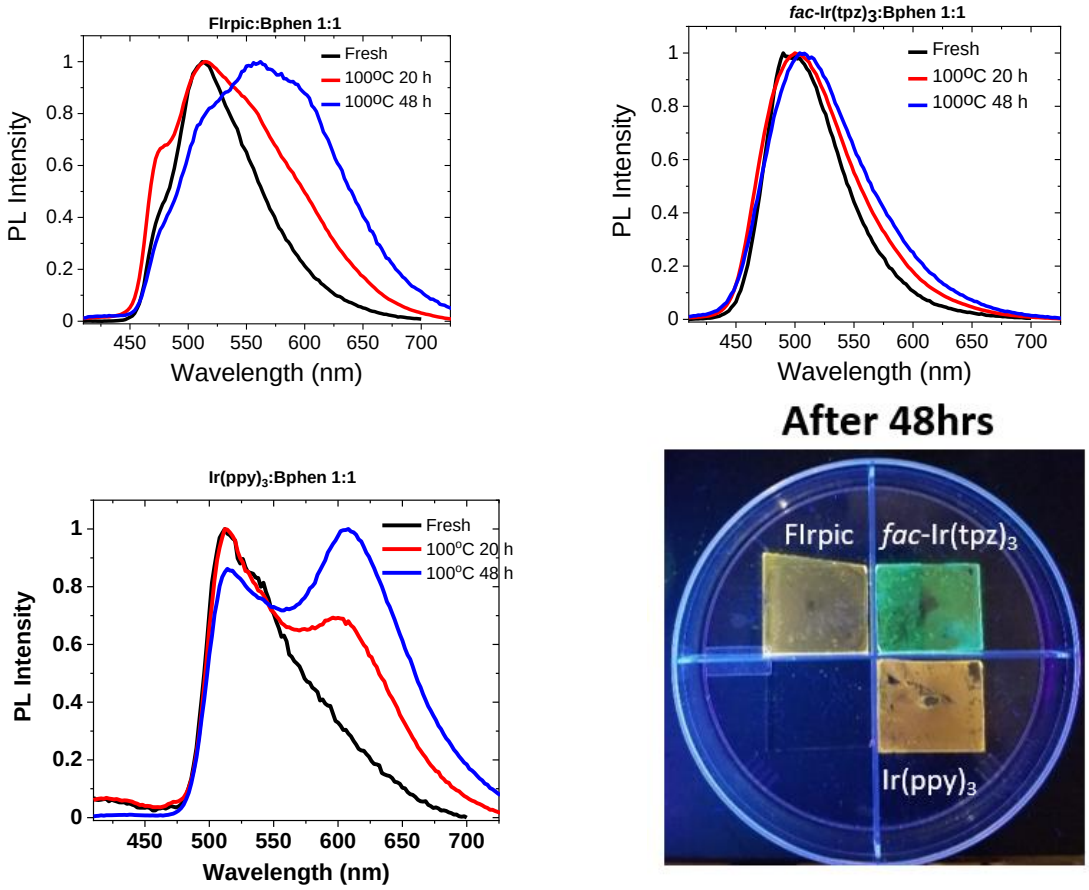

Figure S6. Thermal stability studies of FIrpic, $Ir(tpz)_3$ and $Ir(ppy)_3$ in Bphen.

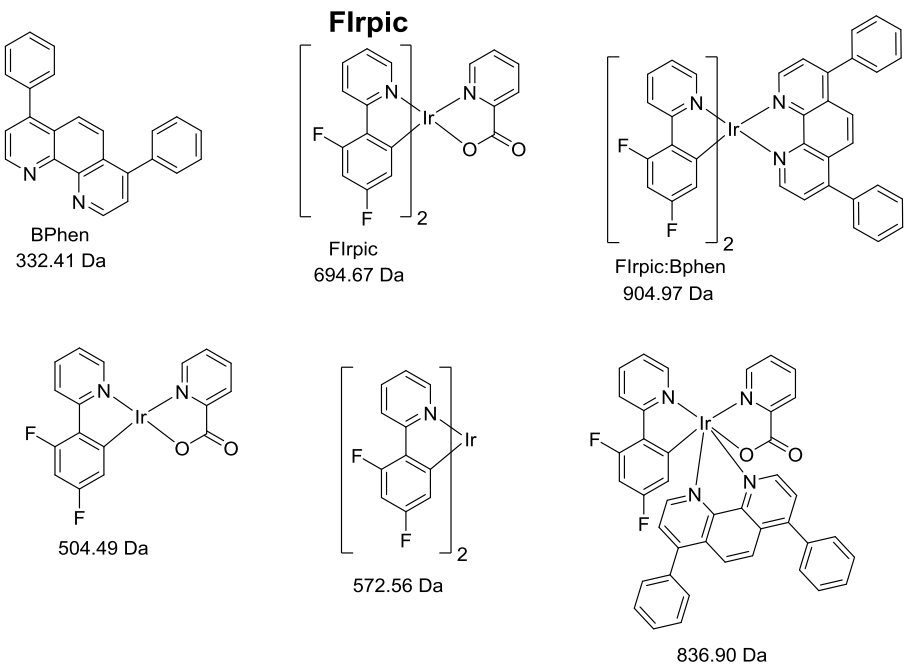

Figure S7. Bphen, FIrpic, and their fragments.

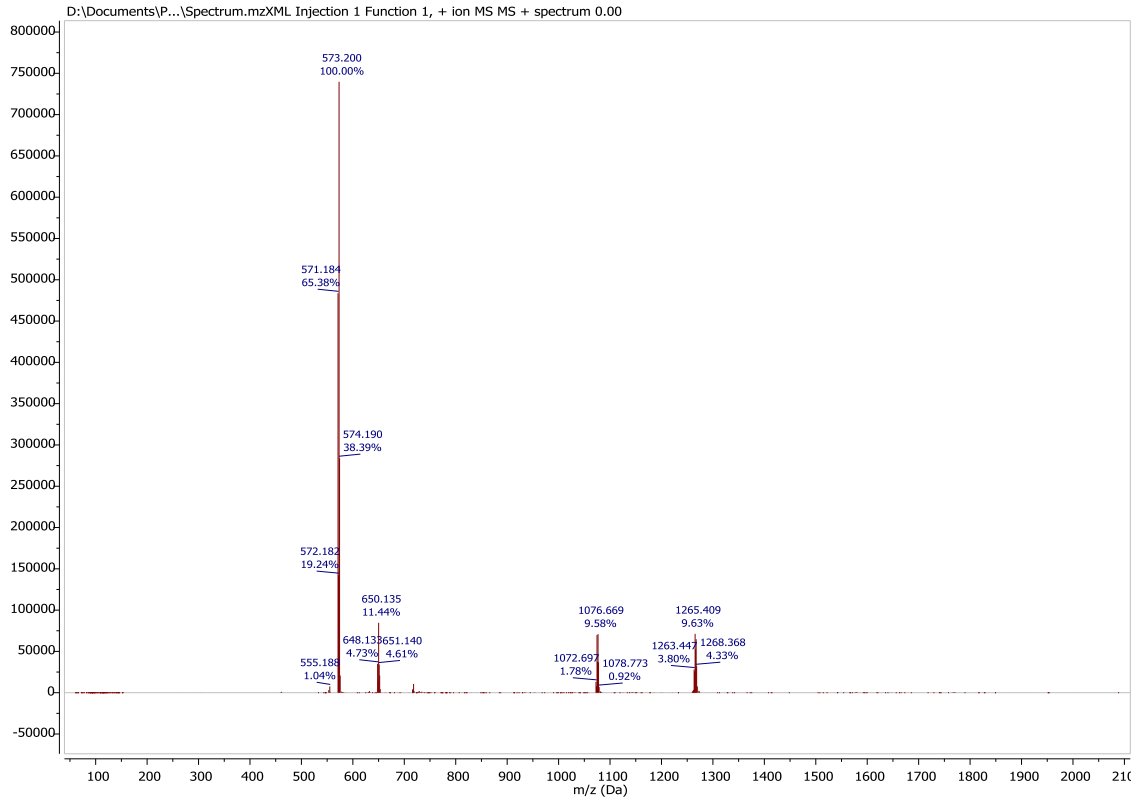

Figure S8. MALDI spectrum of FIrpic film.

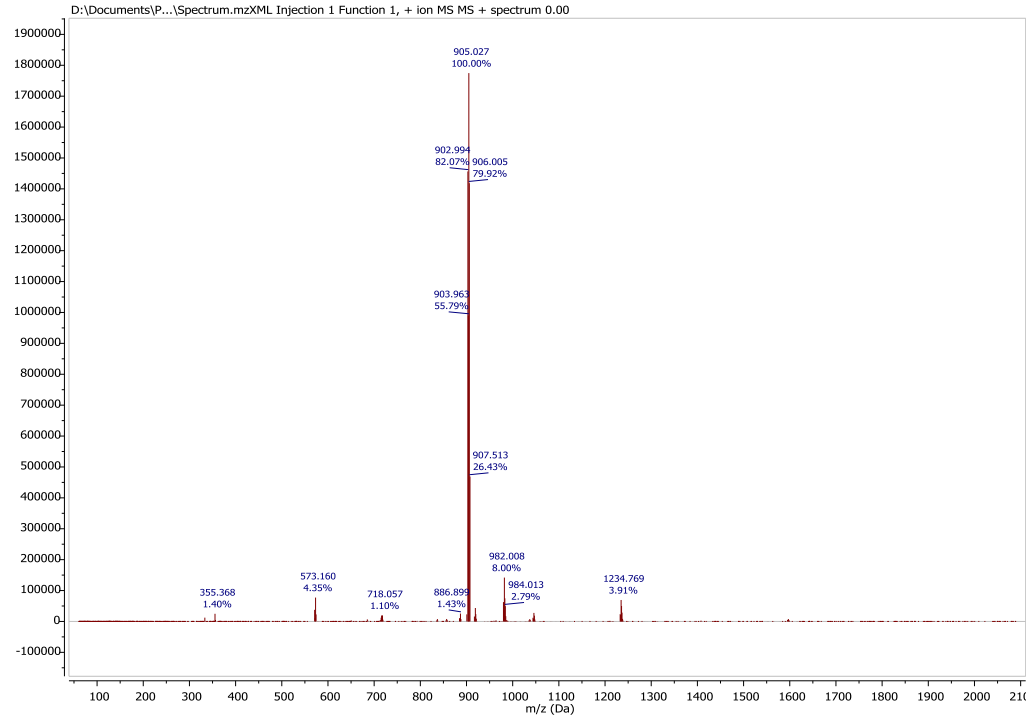

Figure S9. MALDI spectrum of FIrpic:Bphen (1:1) pristine film.

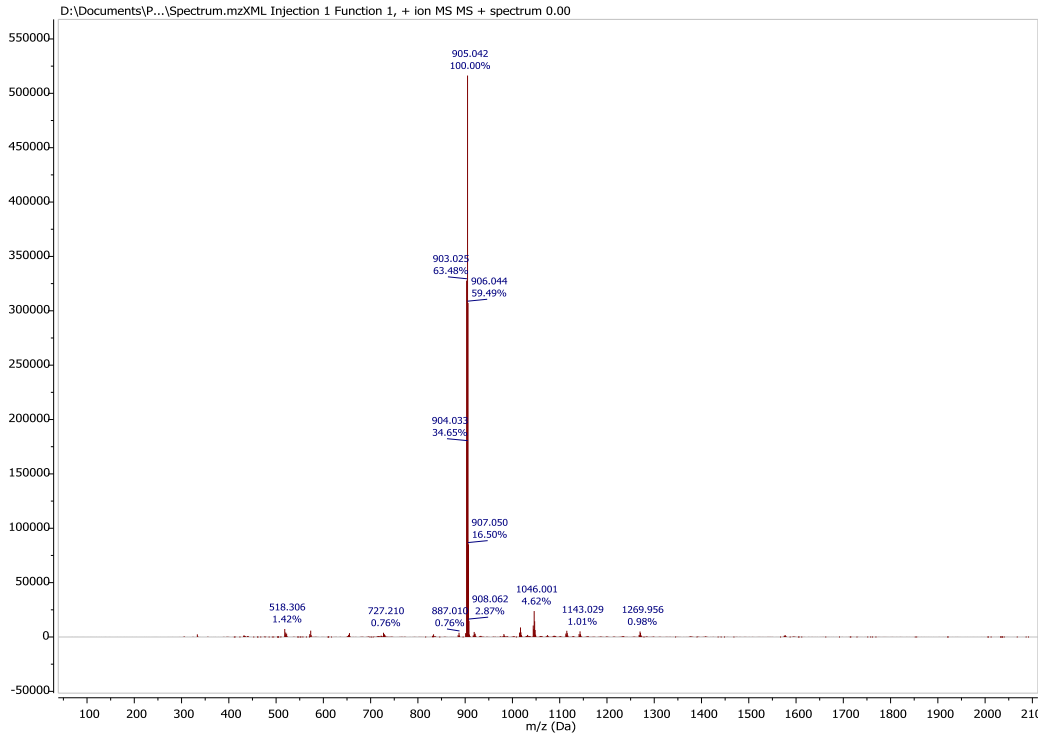

Figure S10. MALDI spectrum of FIrpic:Bphen (1:1) thermally degraded film.

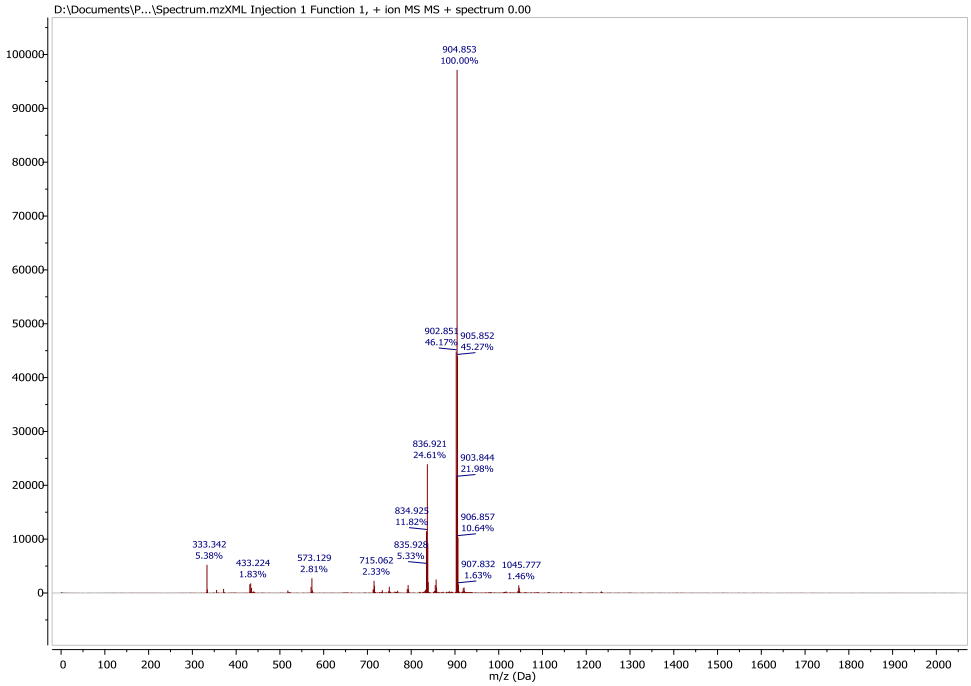

Figure S11. MALDI spectrum of FIrpic:Bphen (1:1) film irradiated with 365 nm light for 48 hours.

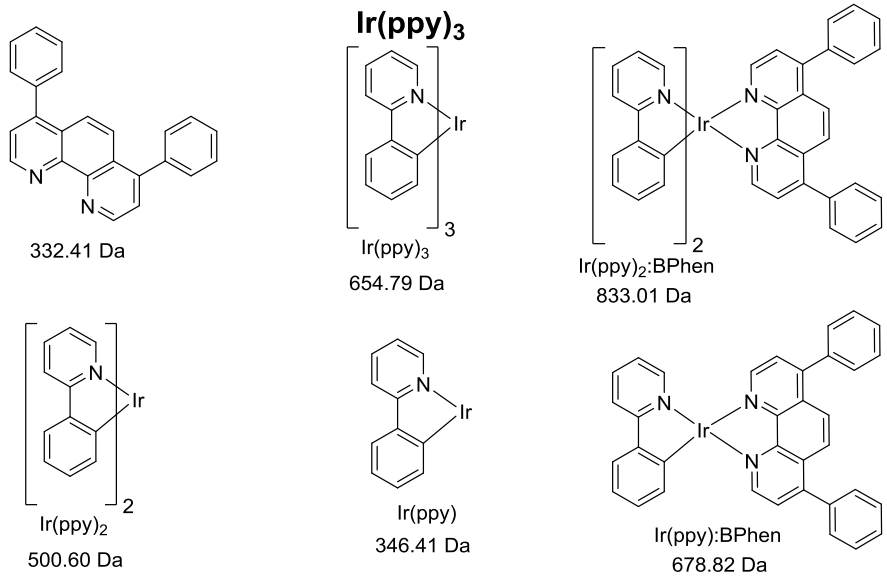

Figure S12. *fac*-Ir(ppy)$_3$, Bphen, and their fragments.

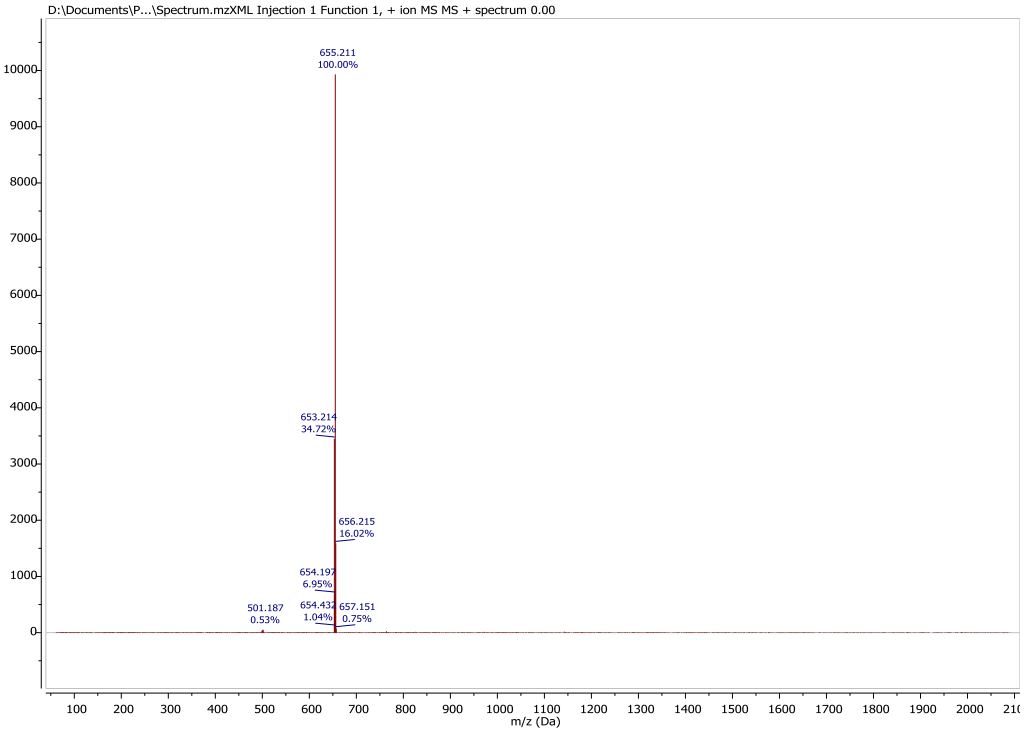

Figure S13. MALDI spectrum of *fac*-Ir(ppy)$_3$ film.

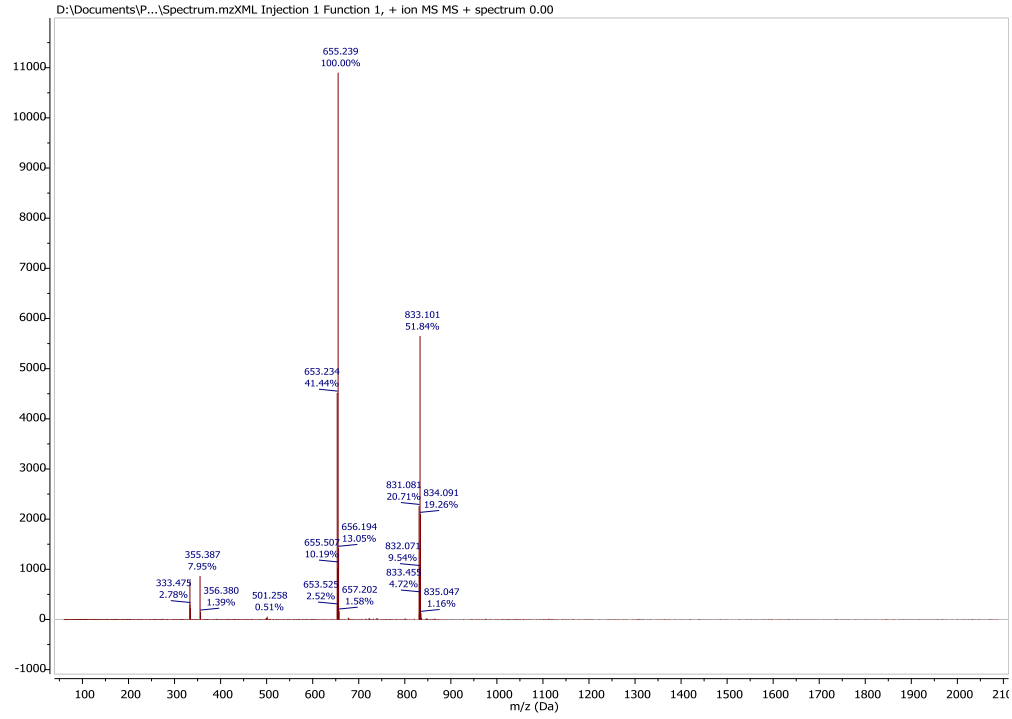

Figure S14. MALDI spectrum of *fac*-Ir(ppy)$_3$:Bphen (1:1) pristine film.

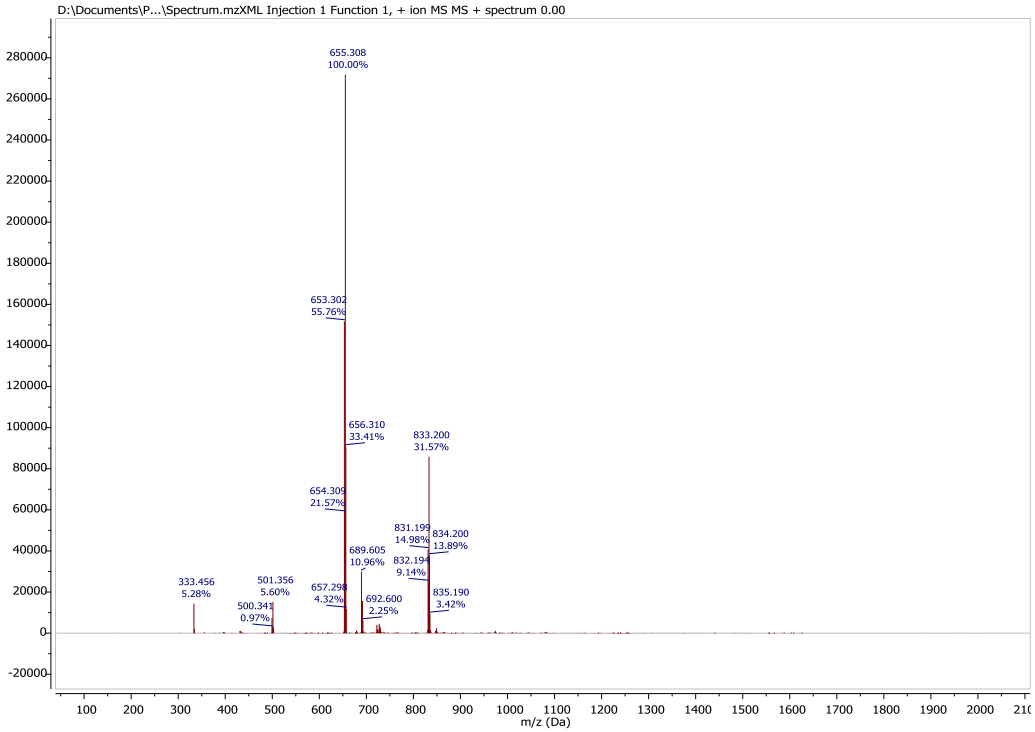

Figure S15. MALDI spectrum of *fac*-Ir(ppy)$_3$:Bphen (1:1) thermally degraded film.

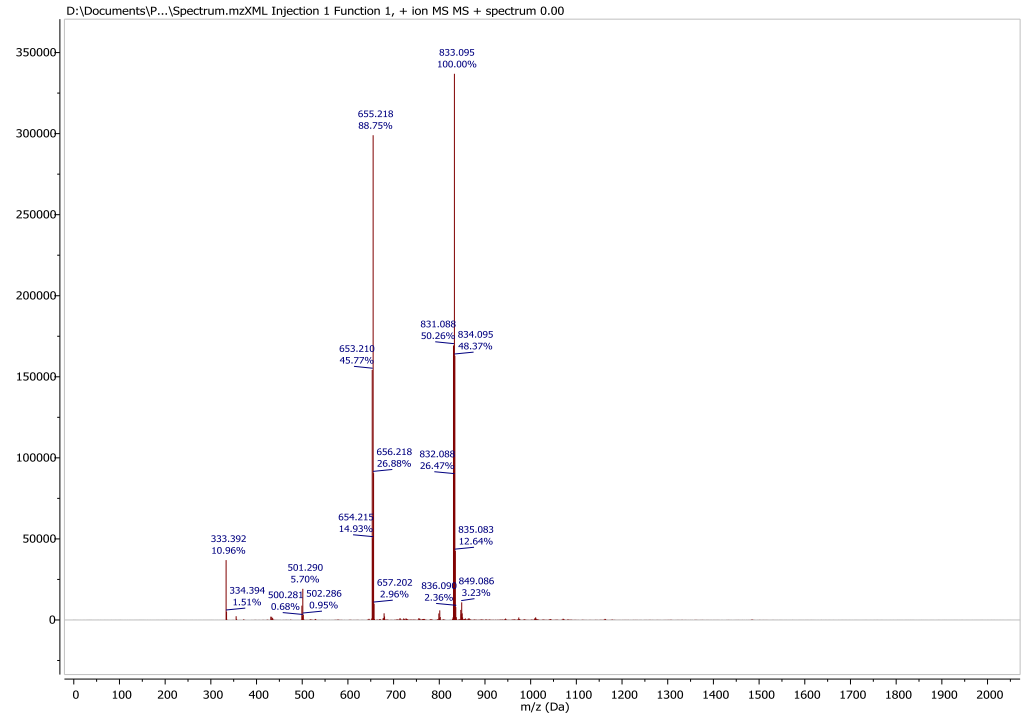

Figure S16. MALDI spectrum of *fac*-Ir(ppy)$_3$:Bphen (1:1) irradiated with 365 nm light for 48 hours.

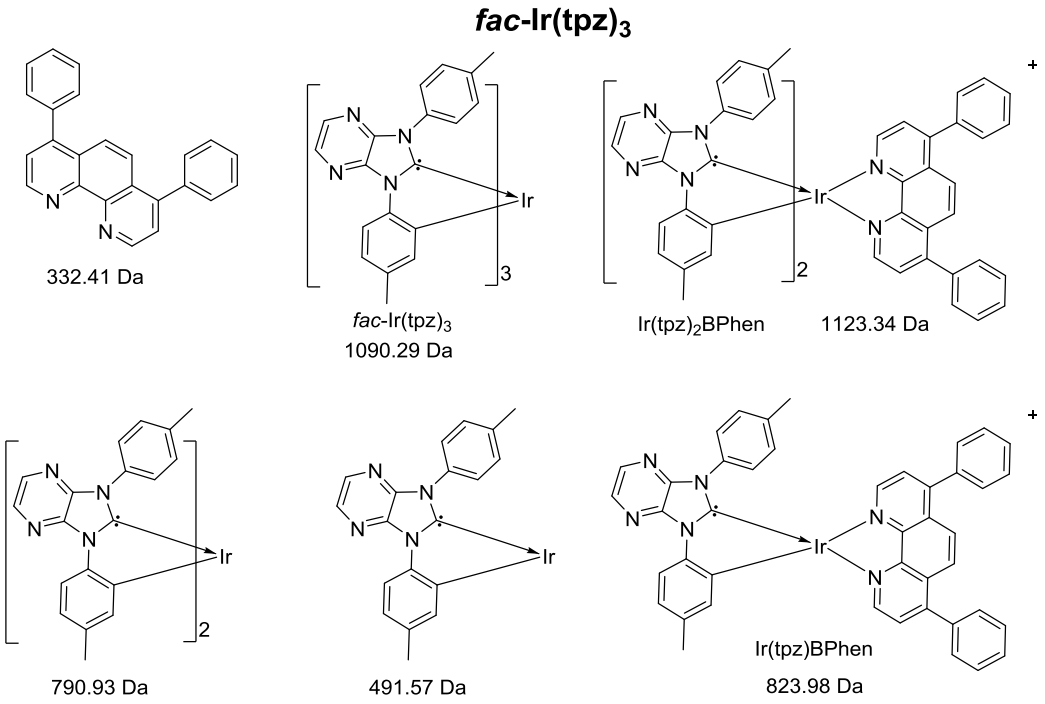

Figure S17. *fac*-Ir(tpz)$_3$, Bphen, and their fragments.

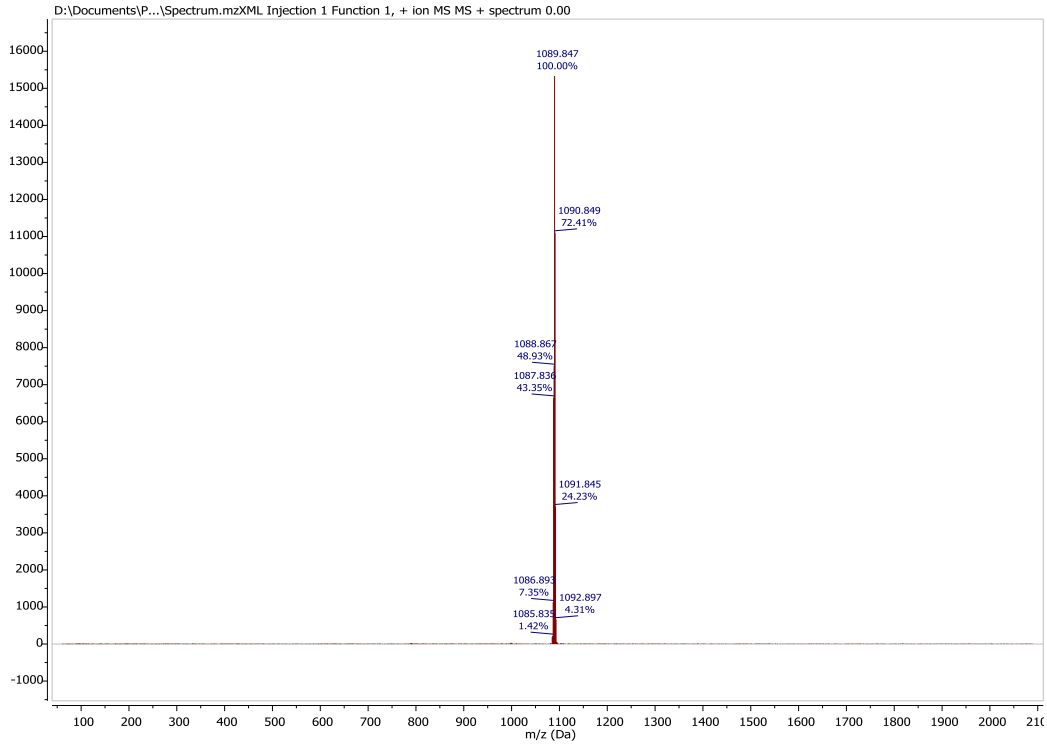

Figure S18. MALDI spectrum of *fac*-Ir(tpz)$_3$ film.

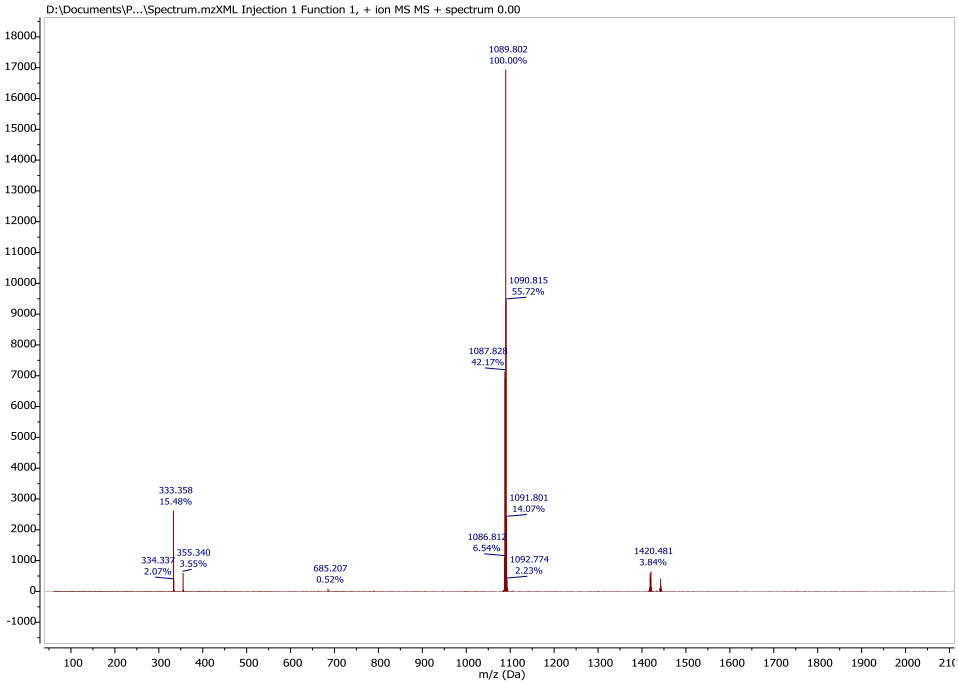

Figure S19. MALDI spectrum of *fac*-Ir(tpz)$_3$:Bphen (1:1) pristine film.

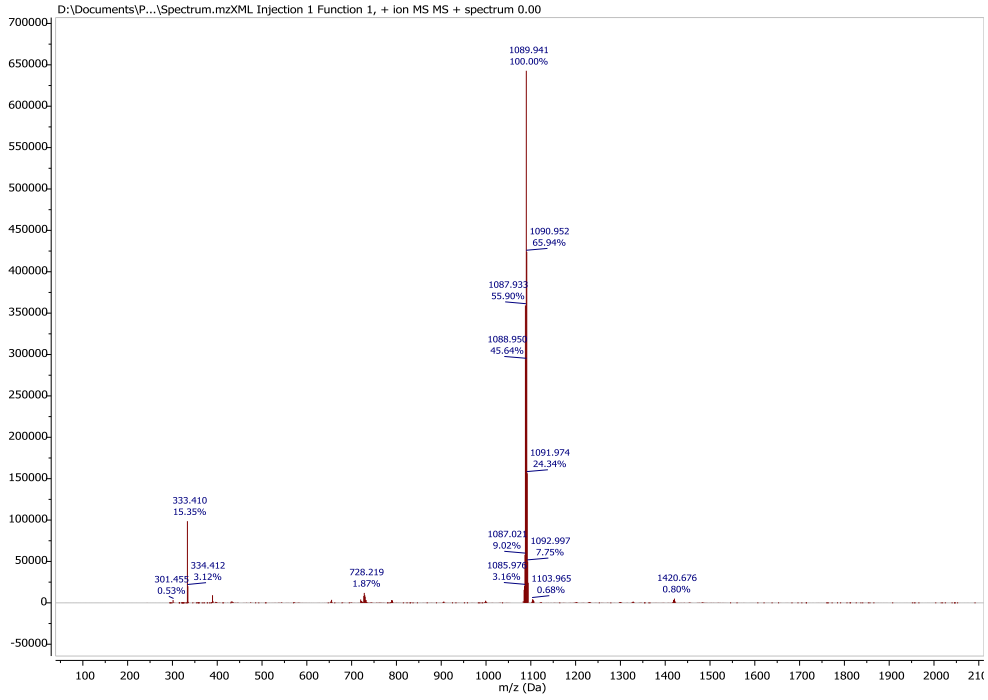

Figure S20. MALDI spectrum of *fac*-Ir(tpz)$_3$:Bphen (1:1) thermally degraded film.

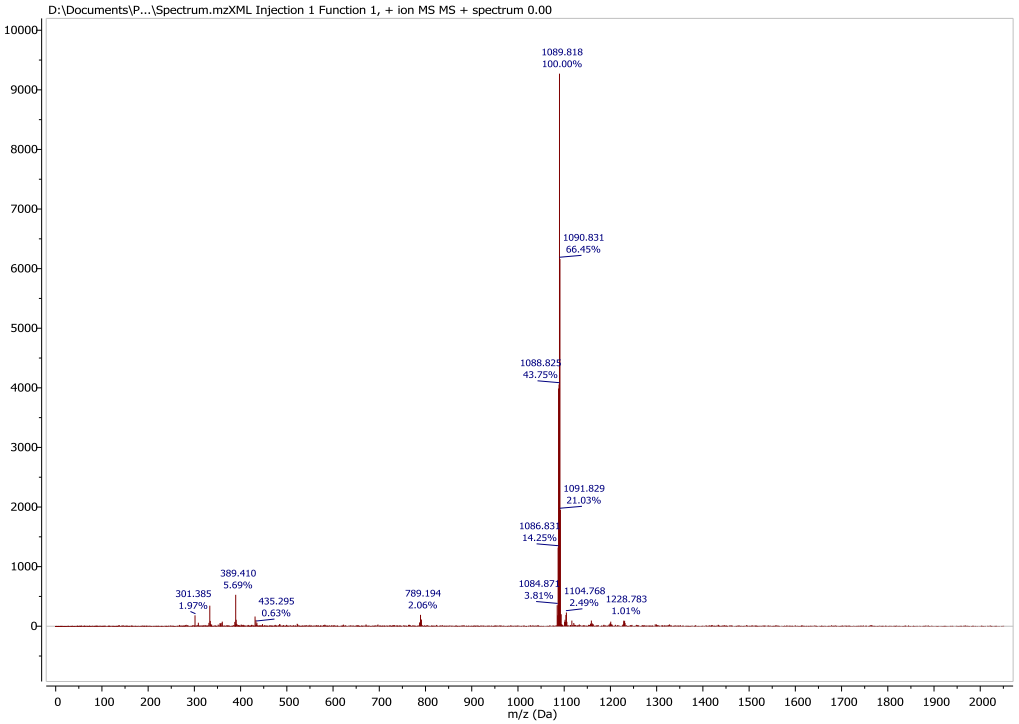

Figure S21. MALDI spectrum of *fac*-Ir(tpz)$_3$:Bphen (1:1)) irradiated with 365 nm light for 48 hours.

Computational Studies

All calculations reported in this work were performed using the Q-Chem 5.2 program.[2] Ground-state optimization calculations were performed using the B3LYP DFT functional and the LACVP** ECP/basis set combination. Time dependent density functional theory (TD-DFT) calculations were used to obtain the excitation energies at the same level.

The extent of overlap (Λ) associated with the electronic transition from the ground state to the S_1 state was computed using the natural transition orbitals (NTOs) according to the following expression:

$$\Lambda = \frac{\sum_k \sigma_k \int |{}^{e}_{k}\phi| \, |{}^{}_{k}\phi| \, d\tau}{\sum_k \sigma_k}$$

where, ${}^{e}_{k}\phi$ and ${}^{}_{k}\phi$ are the electron and hole NTO pairs and σ_k is the amplitude of the corresponding NTO pair. The integrals are computed numerically for each NTO pair using the ORBKIT[3] and Cubature[4] python libraries. An in-house python code was used to compute Λ from the NTOs generated by Q-Chem in Molden format. The source code is available on GitHub (https://github.com/danielsylvinson/OverlApp) and the pre-built binaries (for Windows only) can be downloaded from SourceForge (https://sourceforge.net/projects/overlapp).

The dipole moments of the ground and T_1 states calculated for the complexes are reported in Table S5. The blue and red arrows in Figure 20 denote the dipole moment vectors of the S_0 and T_1 states respectively. The dipole moments indicate strong CT character for the transition in all cases. However, the meridonal isomers exhibit a significantly larger difference in the dipole moment vectors relative to their facial counterparts indicating stronger CT character for the transition. All dipole moment values are reported in Debye.

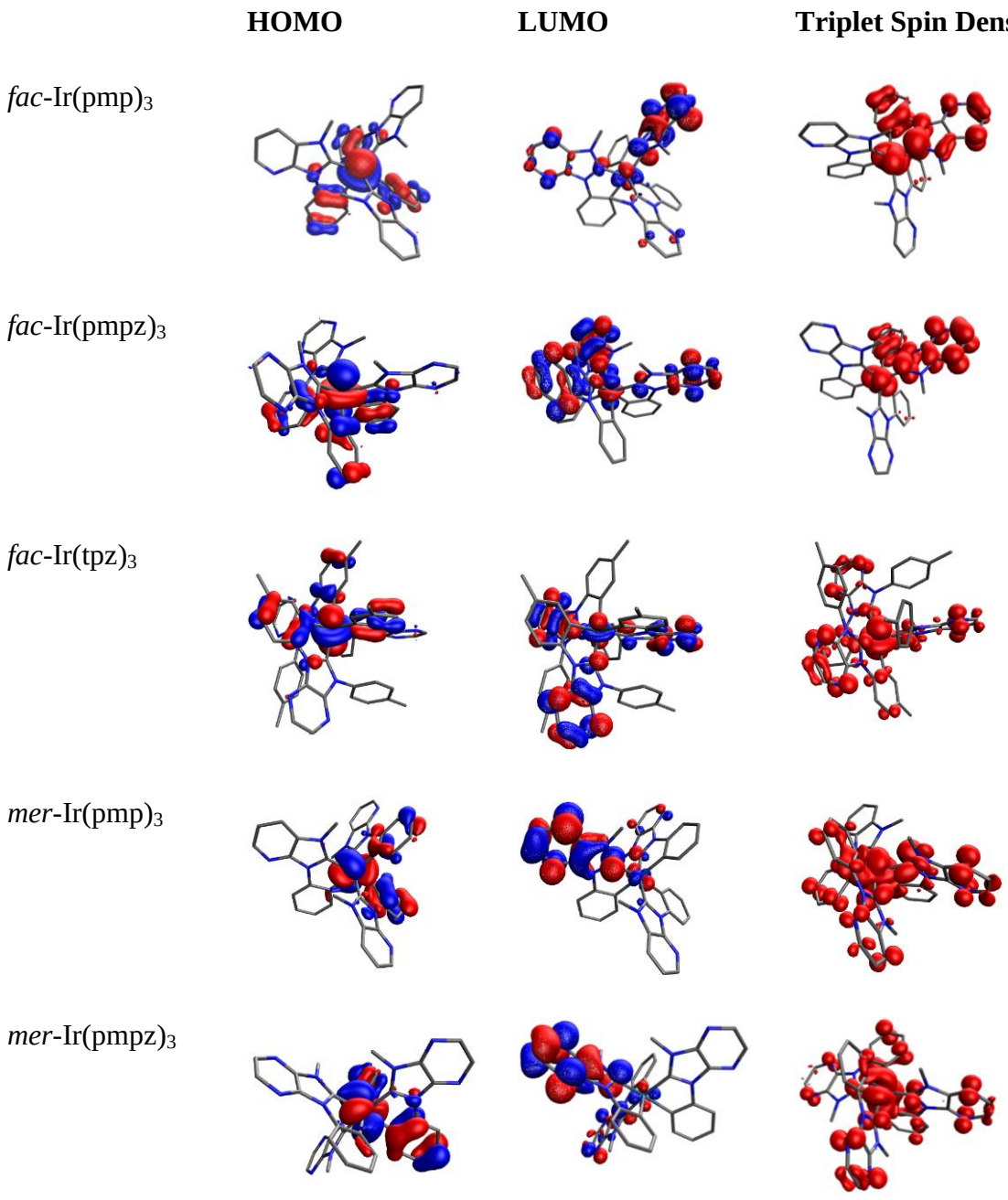

Figure S22. DFT (singlet and triplet, spin density, HOMO and LUMO surfaces)

Table S5. Dipole moments for the S_0 and T_1 of the Ir(C^C:)$_3$ compounds.

complex	μ (S_0)	μ (T_1)	μ' [a]	Δμ' [b]
fac-Ir(tpz)$_3$	7.7	2.3	-2.2	9.9
fac-Ir(pmp)$_3$	11.5	8.4	4.2	7.3
fac-Ir(pmpz)$_3$	7.1	11.3	-2.5	9.6
mer-Ir(pmp)$_3$	7.4	11.4	-10.6	18.0
mer-Ir(pmpz)$_3$	4.5	18.2	-17.3	21.8

[a] μ' is the projection of the dipole moment vector of the T_1 state onto that of the ground state (S_0). Positive values indicate that the dipoles of the two states are oriented along the same direction whereas negative values indicate that they oppose each other. Also, the closer the value of μ' is to μ(T_1), the closer to collinear the two dipoles are. [b] Change in the dipole moment between μ(S_0) and μ'.

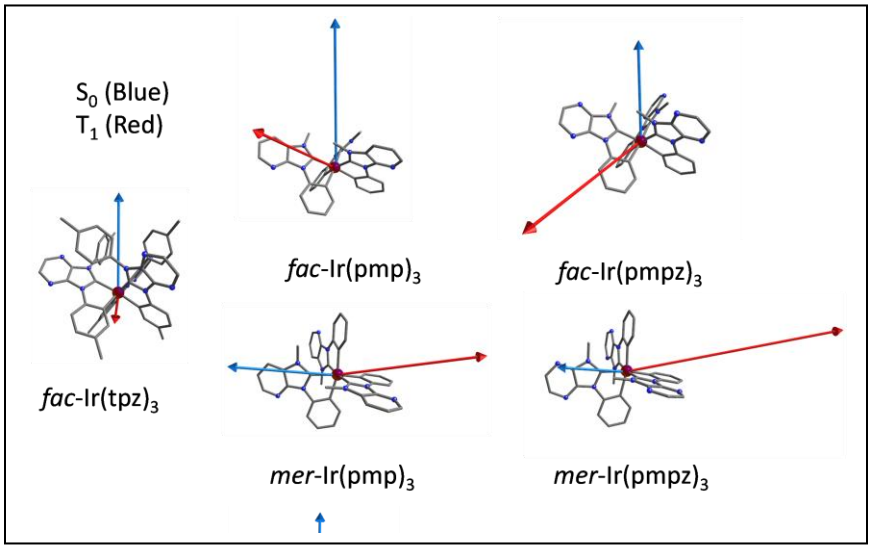

Figure S23. Dipole moment vectors for the S_0 (blue) and T_1 (red) states of the Ir(C^C:)$_3$ compounds.

X-ray Crystallography

Crystal Structure Report for *fac*-Ir(tpz)$_3$

A translucent yellow prism-like specimen of $C_{57}H_{45}IrN_{12}$, approximate dimensions 0.166 mm x 0.170 mm x 0.172 mm, was used for the X-ray crystallographic analysis. The X-ray intensity data were measured on a Bruker APEX DUO system equipped with a TRIUMPH curved-crystal monochromator and a MoKα fine-focus tube (λ = 0.71073 Å).

The total exposure time was 7.00 hours. The frames were integrated with the Bruker SAINT software package using a SAINT V8.37A (Bruker AXS, 2013) algorithm. The integration of the data using a monoclinic unit cell yielded a total of 107868 reflections to a maximum θ angle of 27.48° (0.77 Å resolution), of which 12009 were independent (average redundancy 8.982, completeness = 100.0%, R_{int} = 4.03%, R_{sig} = 2.02%) and 10793 (89.87%) were greater than $2\sigma(F^2)$. The final cell constants of a = 15.232(4) Å, b = 15.340(4) Å, c = 23.660(6) Å, β = 108.728(4)°, volume = 5236.(2) Å^3, are based upon the refinement of the XYZ-centroids of 1015 reflections above 20 σ(I) with 2.792° < 2θ < 57.58°. Data were corrected for absorption effects using the multi-scan method (SADABS). The ratio of minimum to maximum apparent transmission was 0.883. The calculated minimum and maximum transmission coefficients (based on crystal size) are 0.5900 and 0.6700. The structure was solved and refined using the Bruker SHELXTL Software Package, using the space group P 1 21/n 1, with Z = 4 for the formula unit, $C_{57}H_{45}IrN_{12}$. The data was deposited in the Cambridge Crystallographic Database (CCDC #: 2039697). The final anisotropic full-matrix least-squares refinement on F^2 with 637 variables converged at R1 = 2.32%, for the observed data and wR2 = 5.27% for all data. The goodness-of-fit was 1.131. The largest peak in the final difference electron density synthesis was 0.933 e^-/Å^3 and the largest hole was -0.813 e^-/Å^3 with an RMS deviation of 0.077 e^-/Å^3. On the basis of the final model, the calculated density was 1.383 g/cm^3 and F(000), 2192 e^-.

Sample and crystal data for *fac*-Ir(tpz)$_3$.

Identification code	facIrtpz3
Chemical formula	$C_{57}H_{45}IrN_{12}$
Formula weight	1090.25 g/mol
Temperature	100(2) K
Wavelength	0.71073 Å
Crystal size	0.166 x 0.170 x 0.172 mm
Crystal habit	translucent yellow prism
Crystal system	monoclinic
Space group	P 1 21/n 1
Unit cell dimensions	a = 15.232(4) Å $\alpha = 90°$
	b = 15.340(4) Å $\beta = 108.728(4)°$
	c = 23.660(6) Å $\gamma = 90°$
Volume	5236.(2) Å^3
Z	4
Density (calculated)	1.383 g/cm^3
Absorption coefficient	2.599 mm^{-1}
F(000)	2192

Table S6. Data collection and structure refinement for *fac*-Ir(tpz)$_3$

Diffractometer	Bruker APEX DUO
Radiation source	fine-focus tube, MoKα
Theta range for data collection	1.61 to 27.48°
Index ranges	-19<=h<=19, -19<=k<=19, -30<=l<=30
Reflections collected	107868
Independent reflections	12009 [R(int) = 0.0403]
Coverage of independent reflections	100.0%
Absorption correction	multi-scan
Max. and min. transmission	0.6700 and 0.5900
Structure solution technique	direct methods
Structure solution program	SHELXT 2014/5 (Sheldrick, 2014)
Refinement method	Full-matrix least-squares on F^2
Refinement program	SHELXTL XL 2014/7 (Bruker AXS, 2014)
Function minimized	$\Sigma\, w(F_o^2 - F_c^2)^2$
Data / restraints / parameters	12009 / 0 / 637
Goodness-of-fit on F^2	1.131
Δ/σ_{max}	0.005
Final R indices	10793 data; I>2σ(I) R1 = 0.0232, wR2 = 0.0512
	all data R1 = 0.0284, wR2 = 0.0527
Weighting scheme	$w=1/[\sigma^2(F_o^2)+(0.0106P)^2+9.7911P]$ where $P=(F_o^2+2F_c^2)/3$
Largest diff. peak and hole	0.933 and -0.813 eÅ^{-3}
R.M.S. deviation from mean	0.077 eÅ^{-3}

Table S7. Selected Bond Distances (Å) and angles (°) for *fac*-Ir(tpz)$_3$ from Single Crystal XRD (SXRD) and TD-DFT Calculation.

Bond	Bond Distances (Å)		Angles (°)
	SXRD	TDDFT	SXRD
Ir-C$_{(carbene)}$			
Ir1-C1	2.027(2)	2.061	
Ir1-C20	2.027(2)	2.061	
Ir1-C39	2.028(2)	2.061	
Ir-C$_{(tolyl)}$			
Ir-C14	2.090(2)	2.108	
Ir1-C33	2.087(2)	2.108	
Ir1-C52	2.096(2)	2.108	
C$_{(carbene1)}$-Ir- C$_{(carbene2)}$			
C1-Ir1-C20			96.2(1)
C1-Ir1-C39			104.3(1)

NMR Data

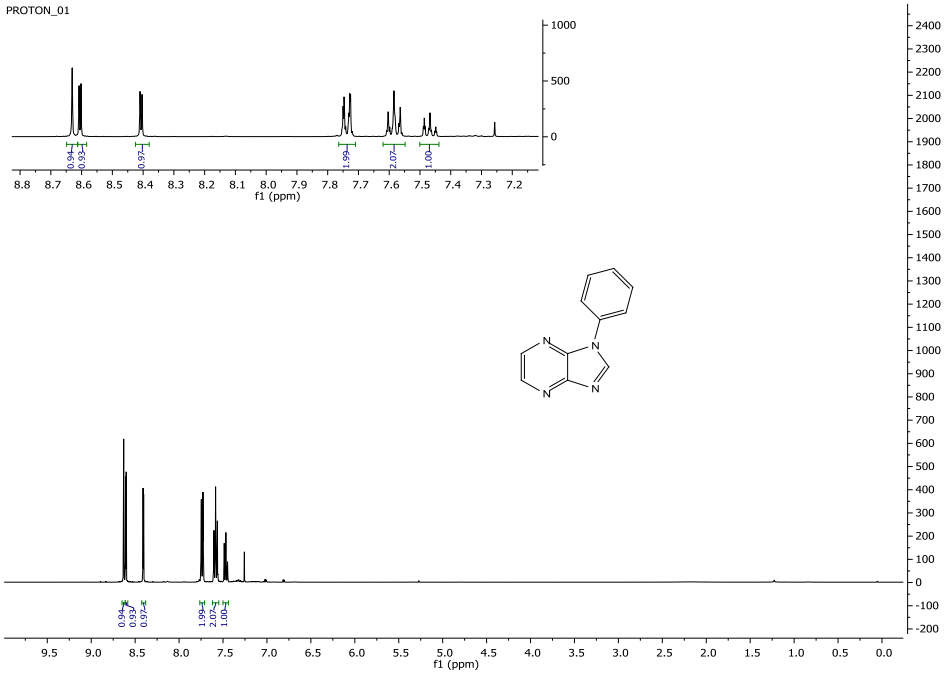

Figure S24. ^{1}H-NMR of **3** in $CDCl_3$.

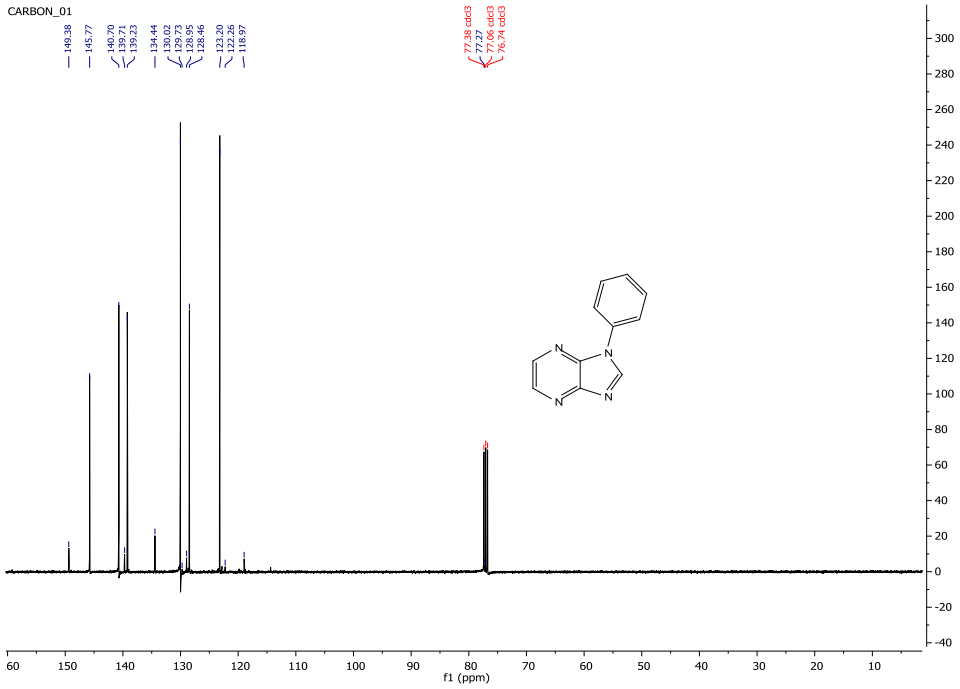

Figure S25. ^{13}C-NMR of **3** in $CDCl_3$.

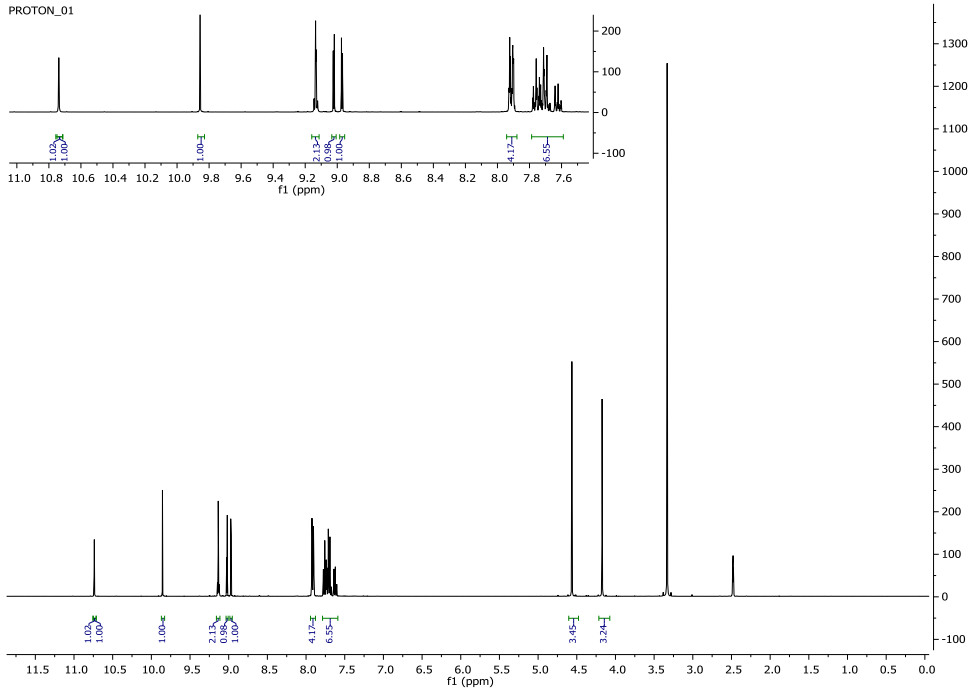

Figure S26. ^{1}H-NMR of a mixture of **4** and byproduct in DMSO-d_6.

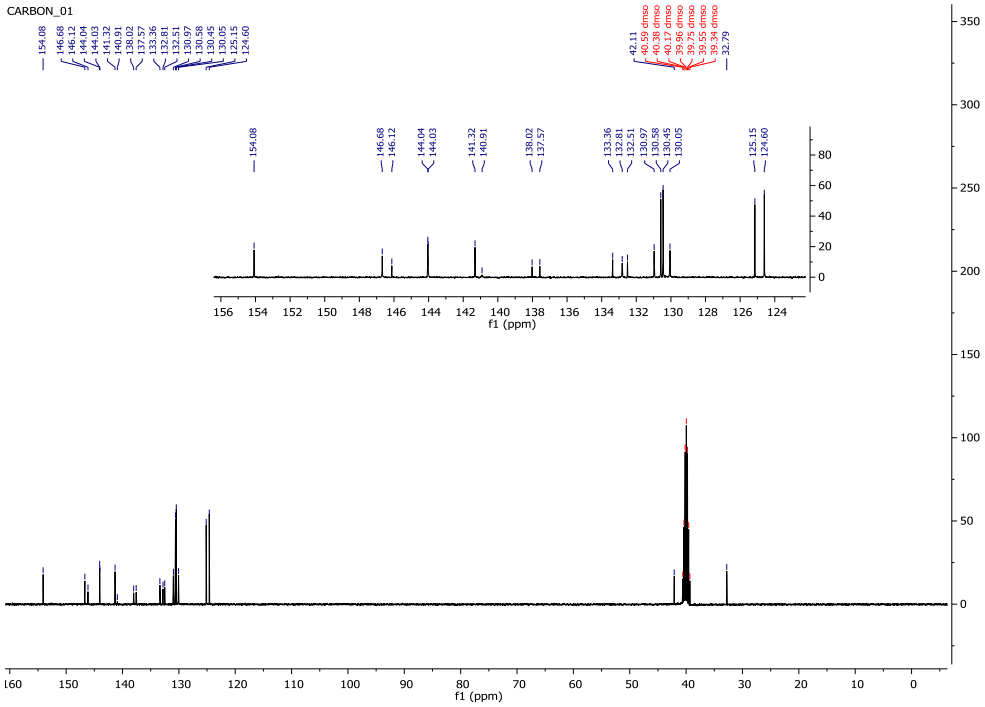

Figure 27. ^{13}C-NMR of a mixture of **4** and byproduct in DMSO-d_6.

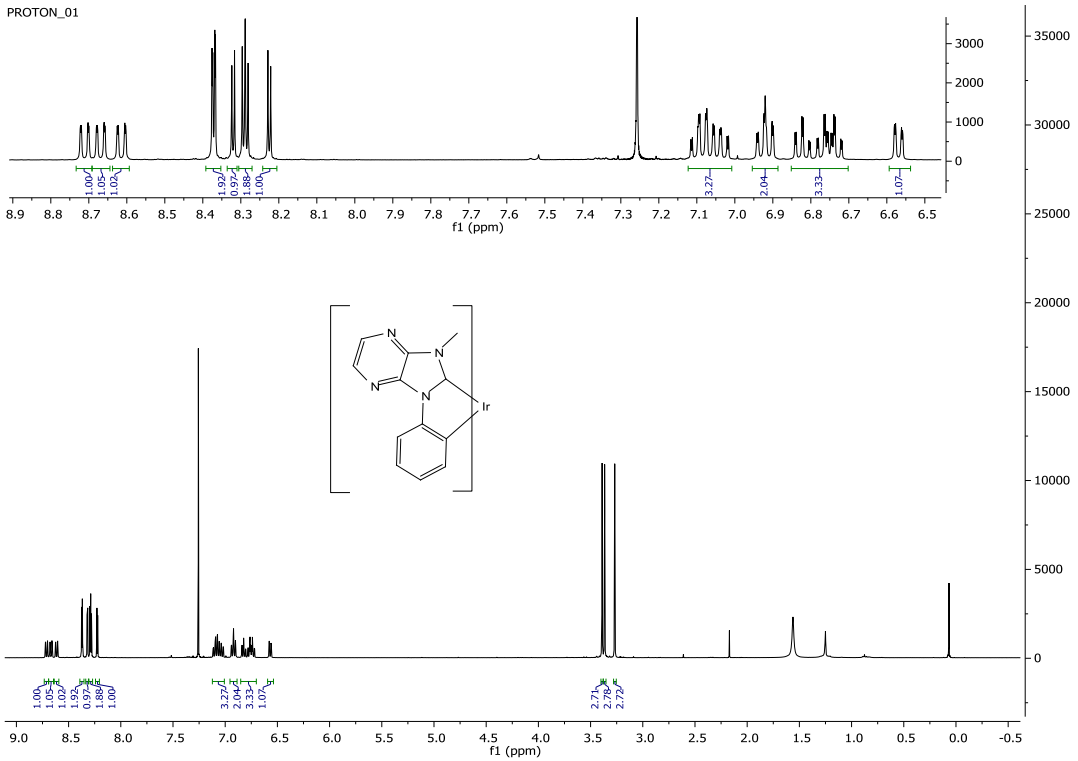

Figure S28. ^{1}H-NMR of *mer*-Ir(pmpz)$_3$ in CDCl$_3$.

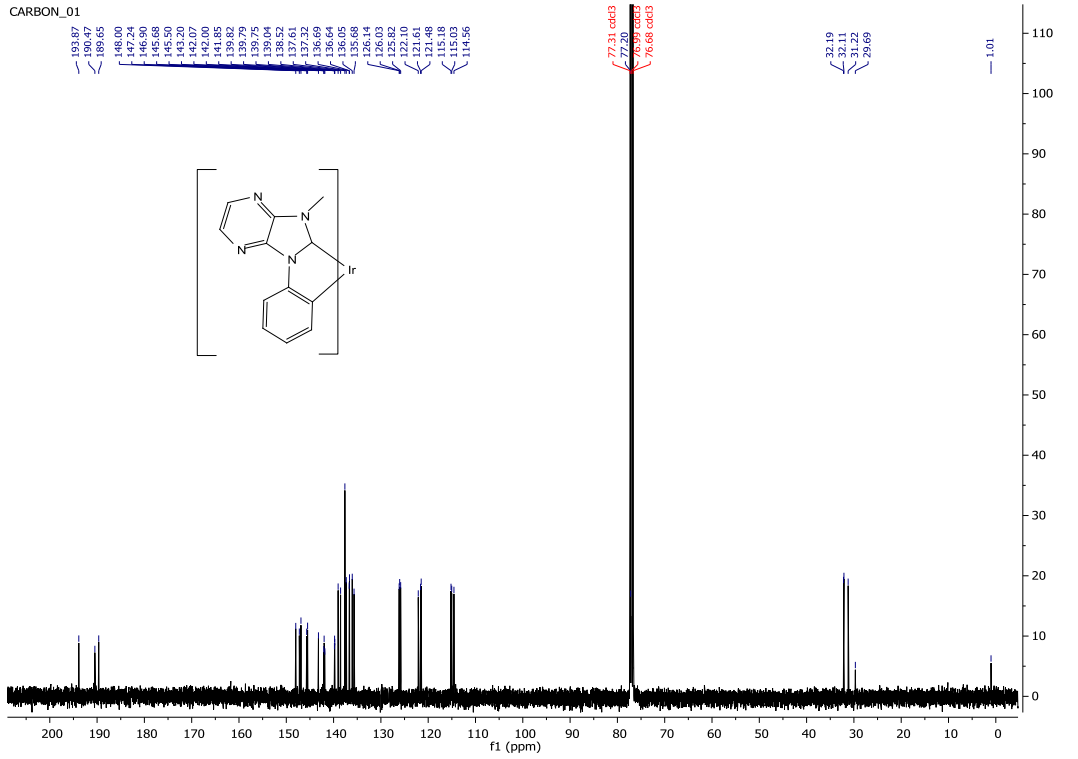

Figure S29. ^{13}C-NMR of *mer*-Ir(pmpz)$_3$ in CDCl$_3$.

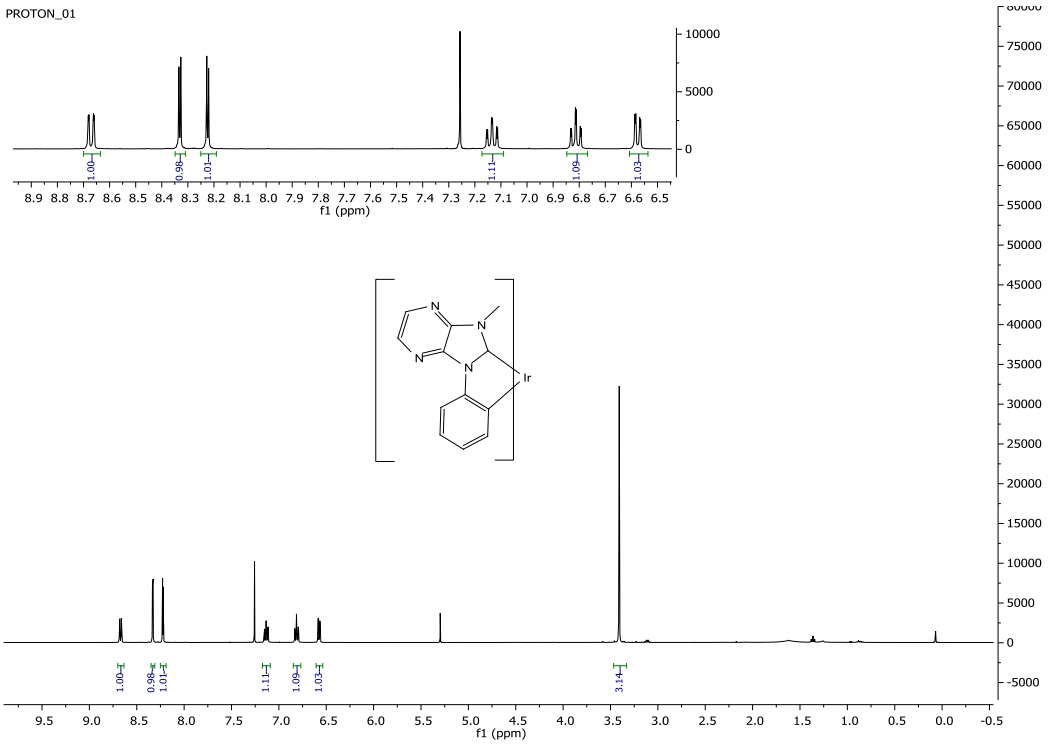

Figure S30. ^{1}H-NMR of *fac*-Ir(pmpz)$_3$ in $CDCl_3$.

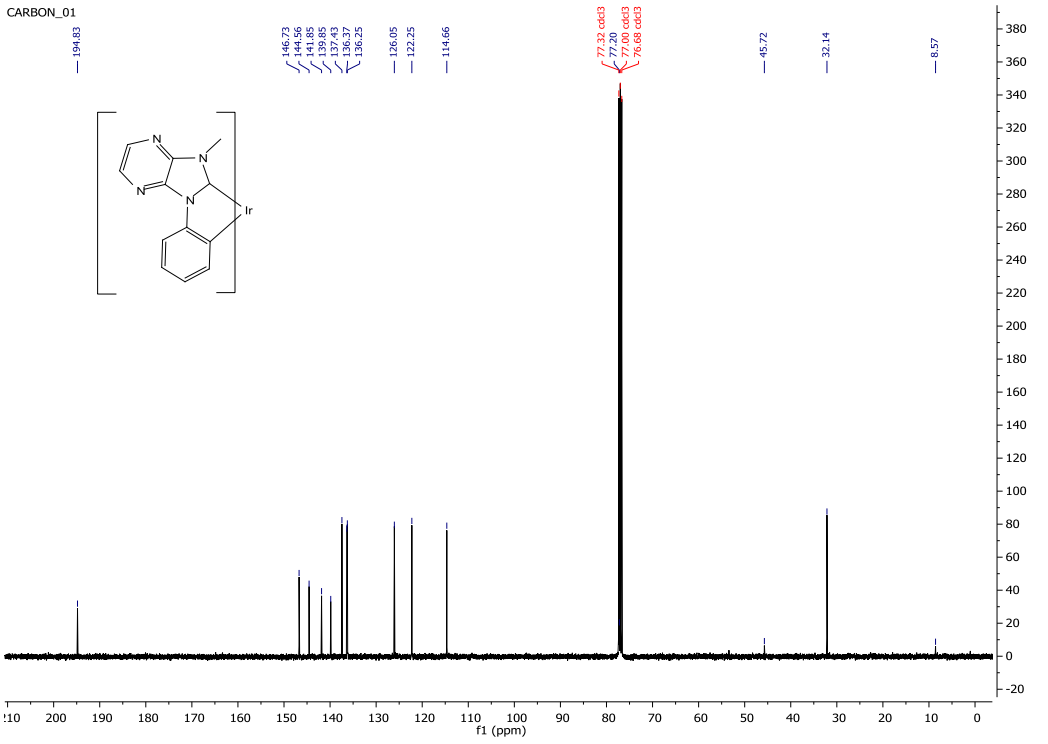

Figure S31. ^{13}C-NMR of *fac*-Ir(pmpz)$_3$ in $CDCl_3$.

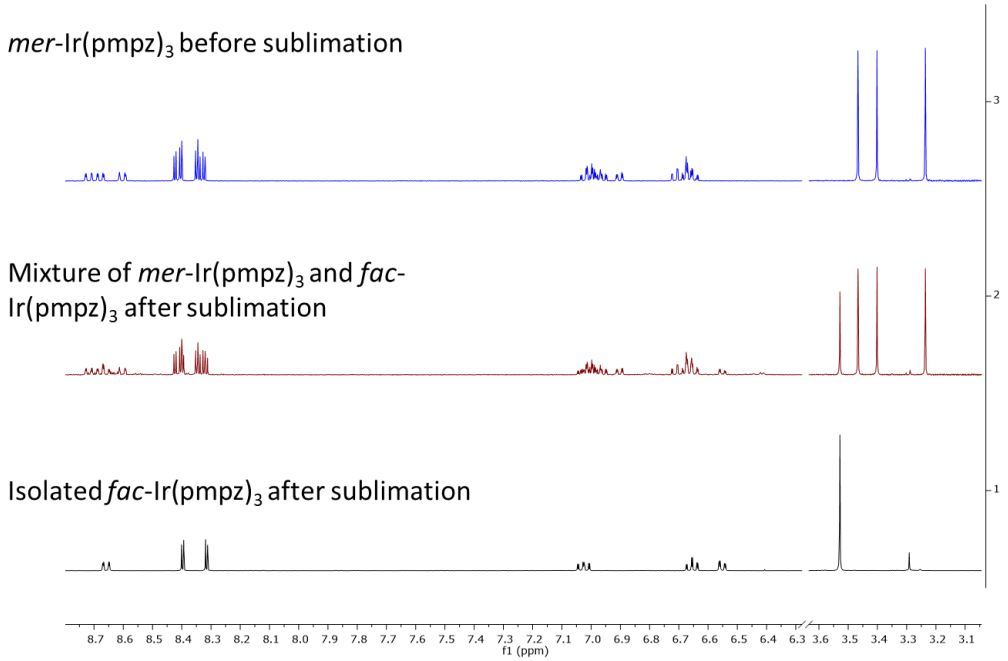

Figure S32. ^{1}H-NMR of *mer*-Ir(pmpz)$_3$ before sublimation (blue), after sublimation (red) and isolated *fac*-Ir(pmpz)$_3$ in Acetone-d$_6$. Sublimation conditions: 330 °C (zone 1), 250 °C (zone 2), 100 °C (zone 3). Pressure: 2.5 x 10^{-6} Torr.

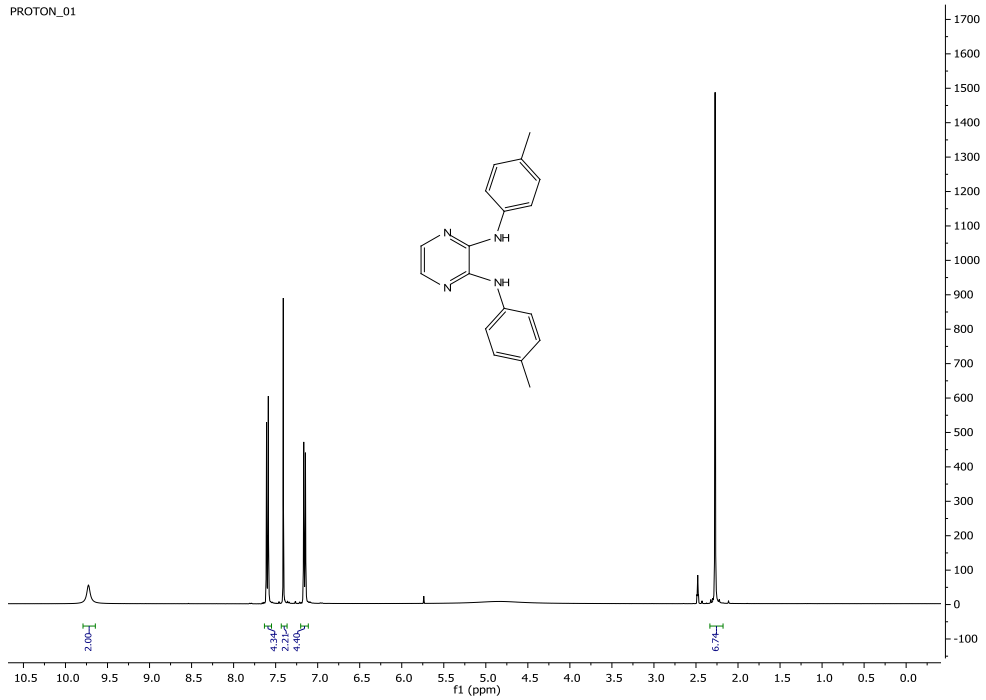

Figure S33. ^{1}H-NMR of **5** in DMSO-d$_6$.

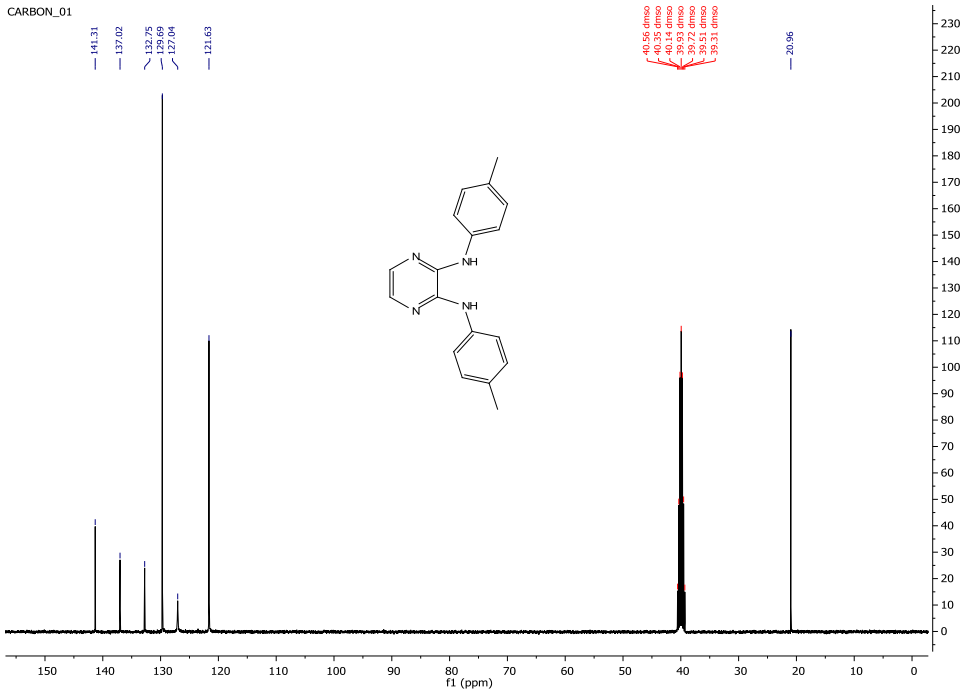

Figure S34. ^{13}C-NMR of **5** in DMSO-d_6.

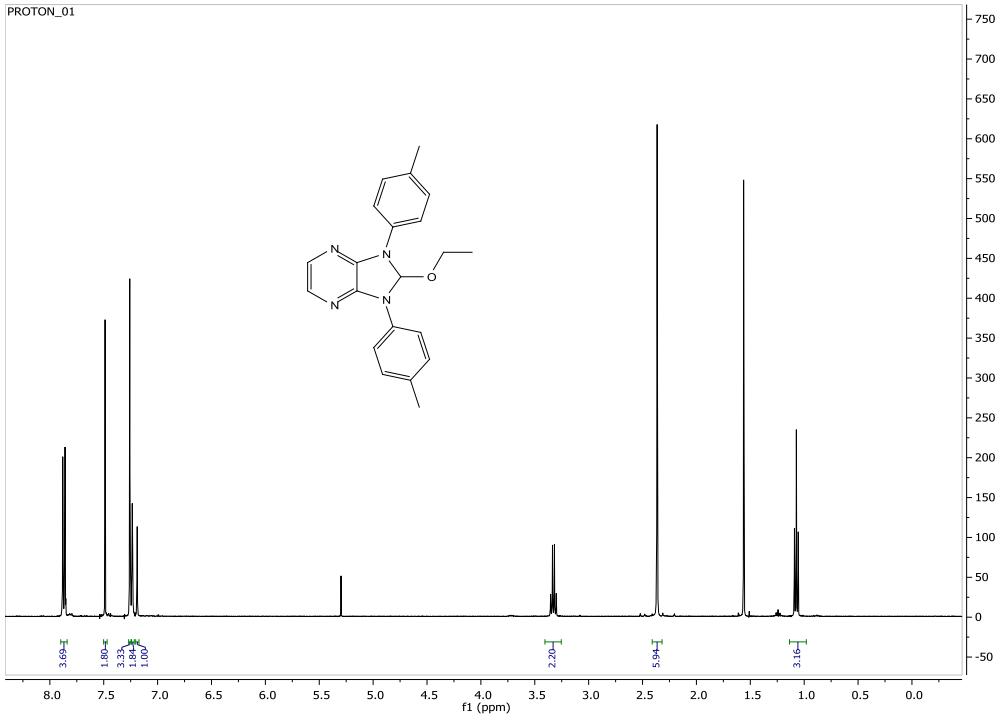

Figure 35. ^{1}H-NMR of **6** in $CDCl_3$.

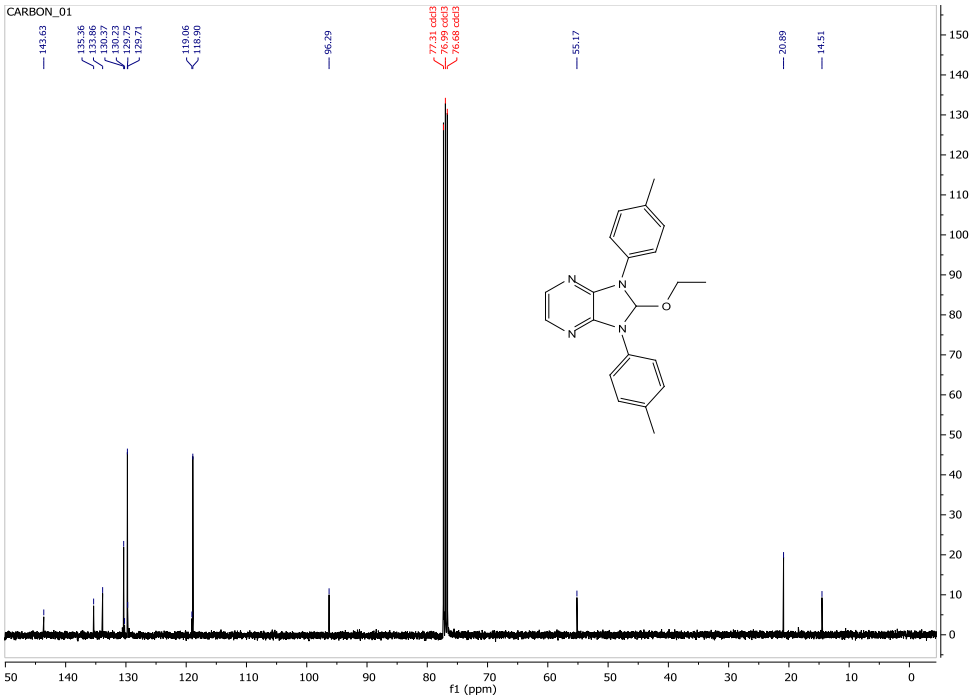

Figure S36. ^{13}C-NMR of **6** in $CDCl_3$.

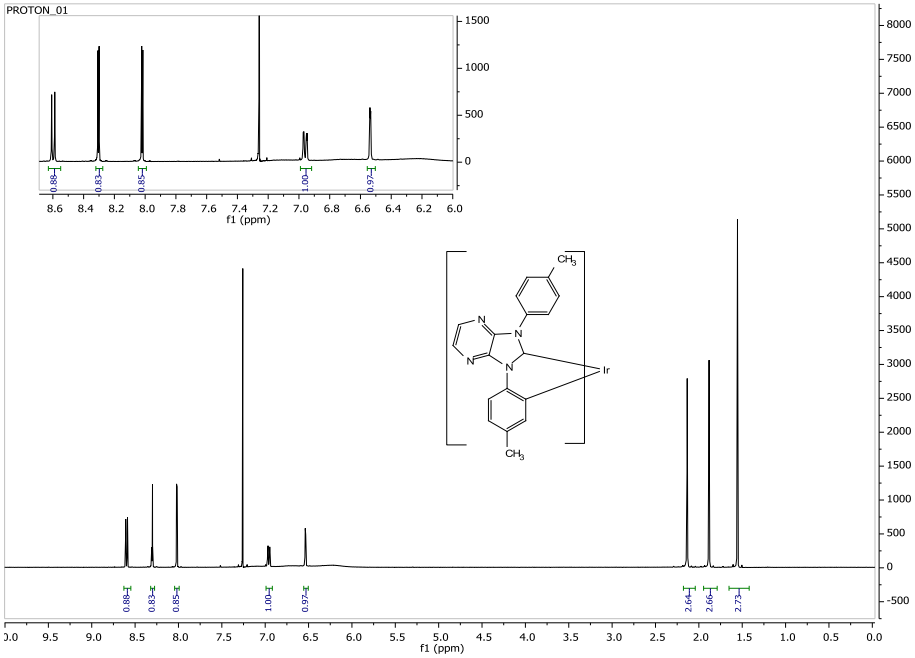

Figure S37. ^{1}H-NMR of *fac*-Ir(tpz)$_3$ in $CDCl_3$.

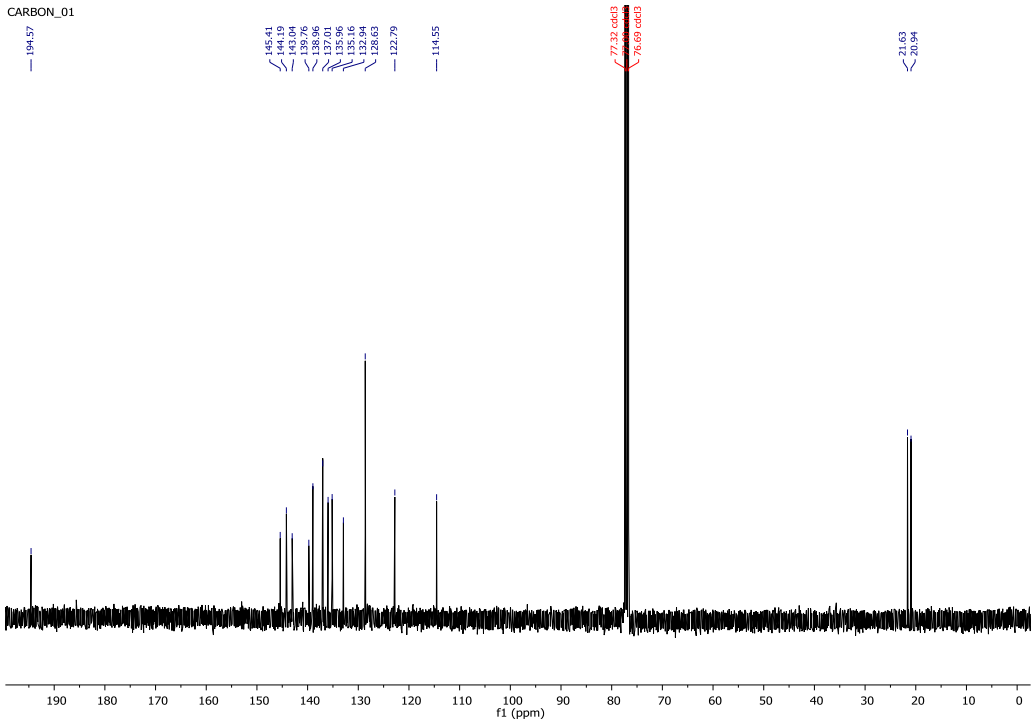

Figure S38. ^{13}C-NMR of *fac*-Ir(tpz)$_3$ in $CDCl_3$.

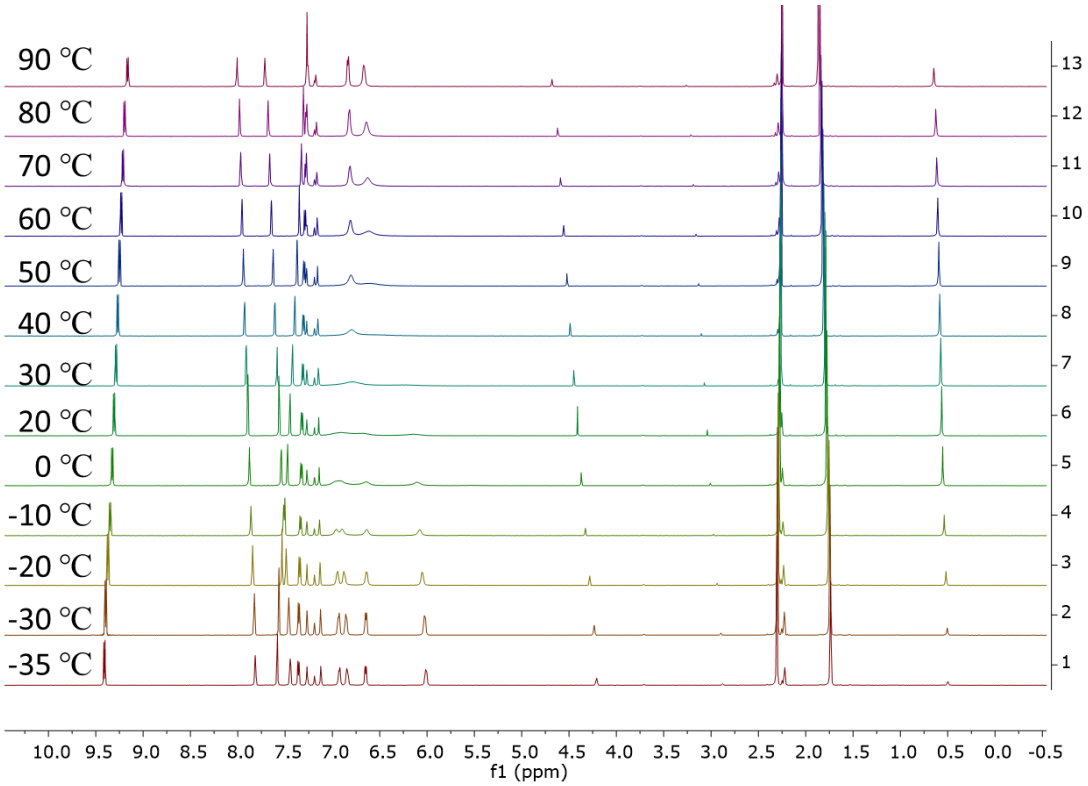

Figure S39. Variable temperature ^{1}H-NMR of *fac*-Ir(tpz)$_3$ in Toluene-d_8.

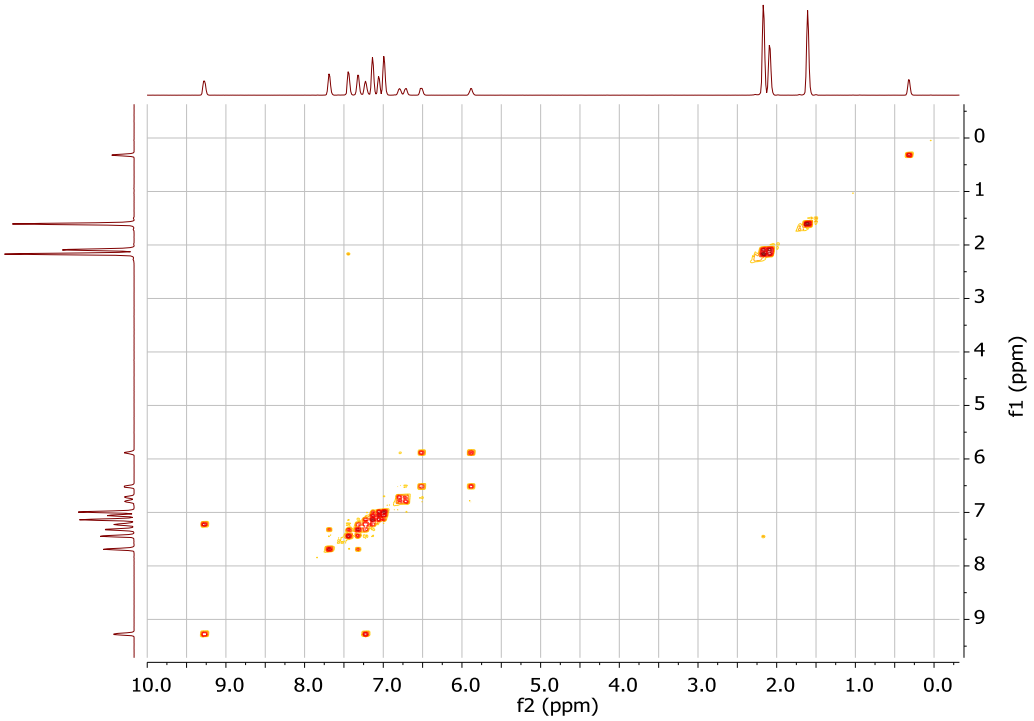

Figure S40. COSY-NMR of *fac*-Ir(tpz)$_3$ in Toluene-d$_8$ at -34 °C.

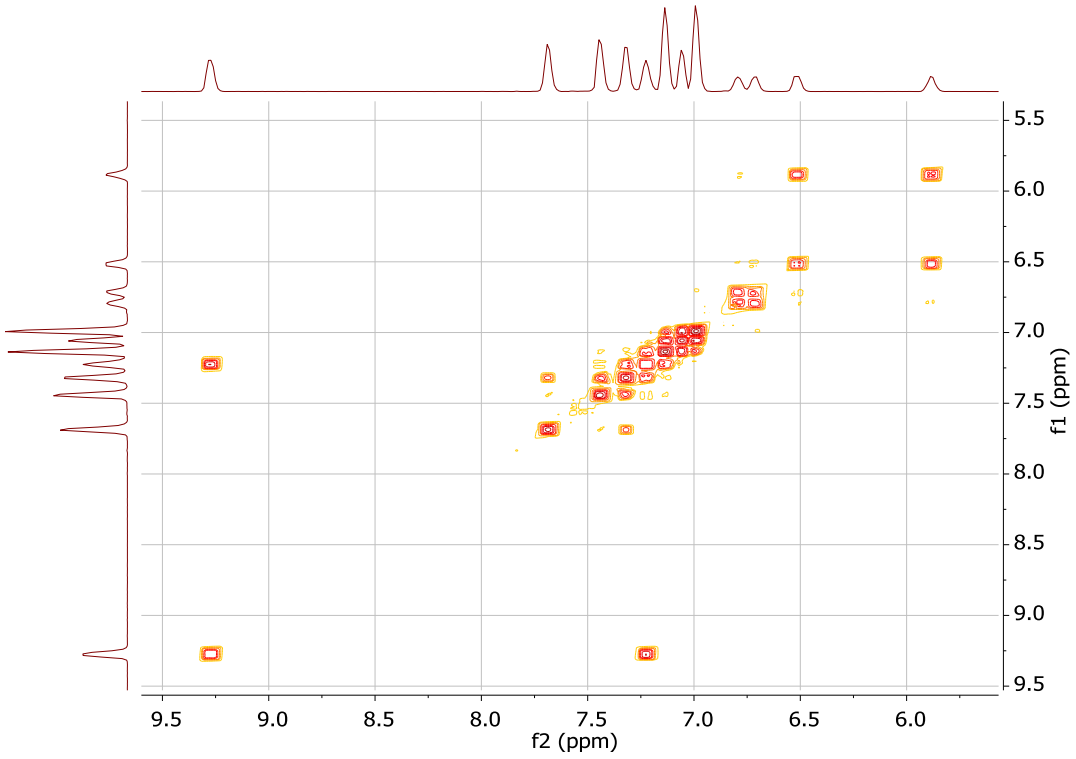

Figure S41. COSY-NMR of *fac*-Ir(tpz)$_3$ in Toluene-d$_8$ (aromatic region) at -34 °C.

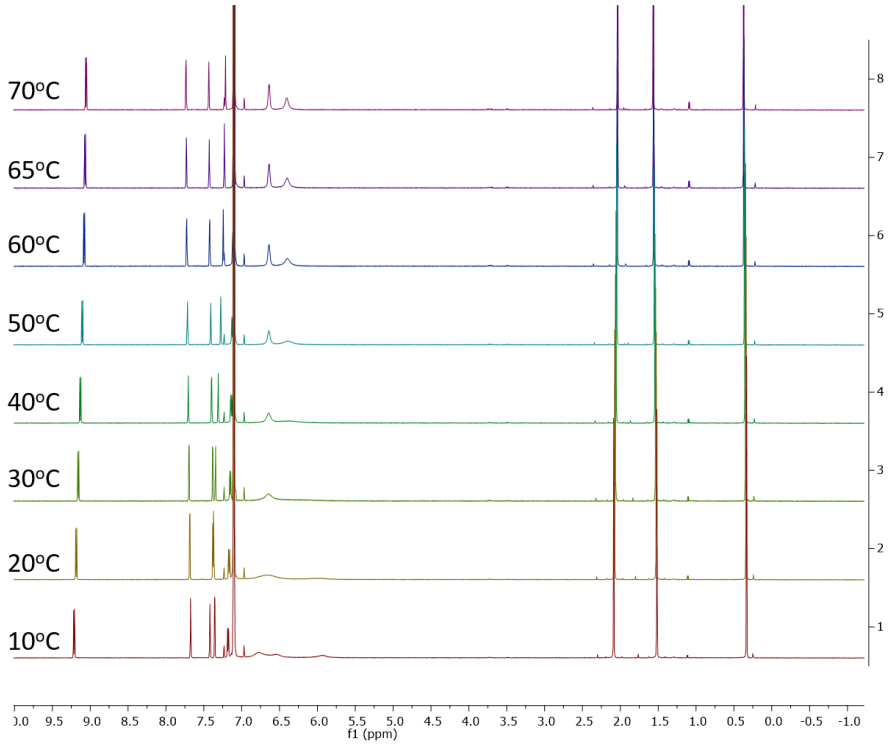

Figure S42. Variable temperature ^{1}H-NMR of *fac*-Ir(tpz)$_3$ in Benzene-d$_6$.

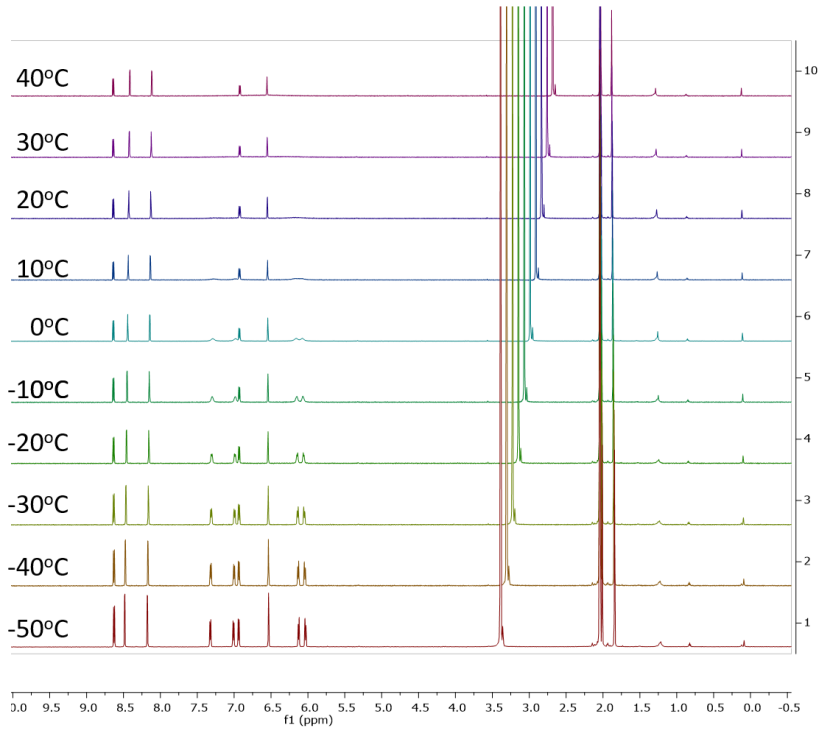

Figure S43. Variable temperature ^{1}H-NMR of *fac*-Ir(tpz)$_3$ in Acetone-d$_6$.

Mass Spectral Data

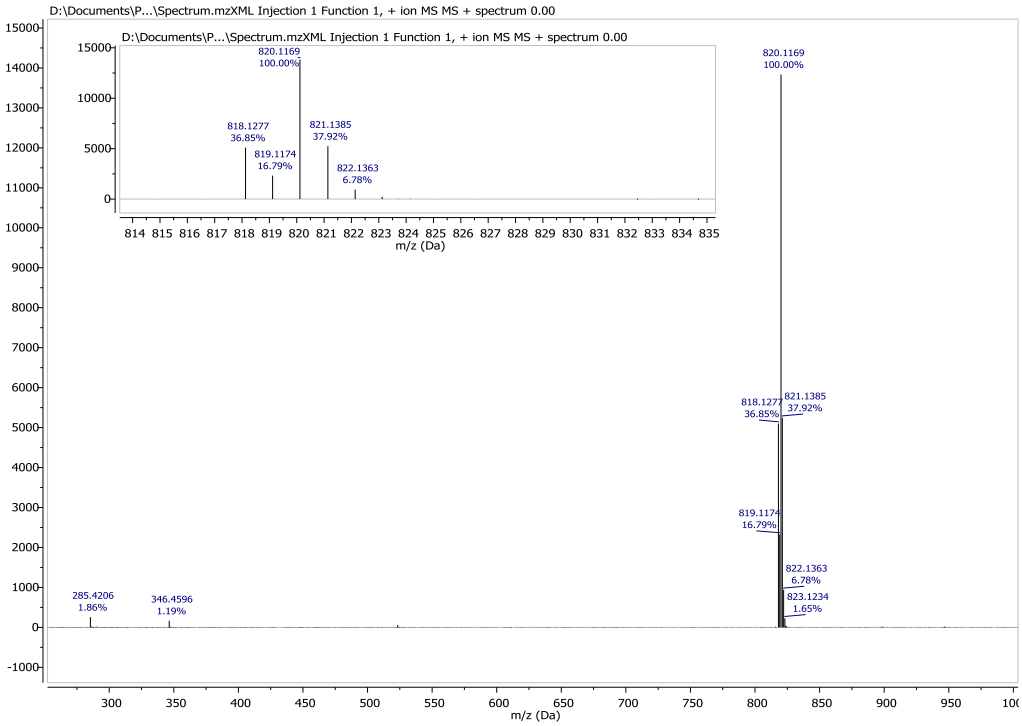

Figure S44. MALDI spectrum of *fac*-Ir(pmpz)$_3$.

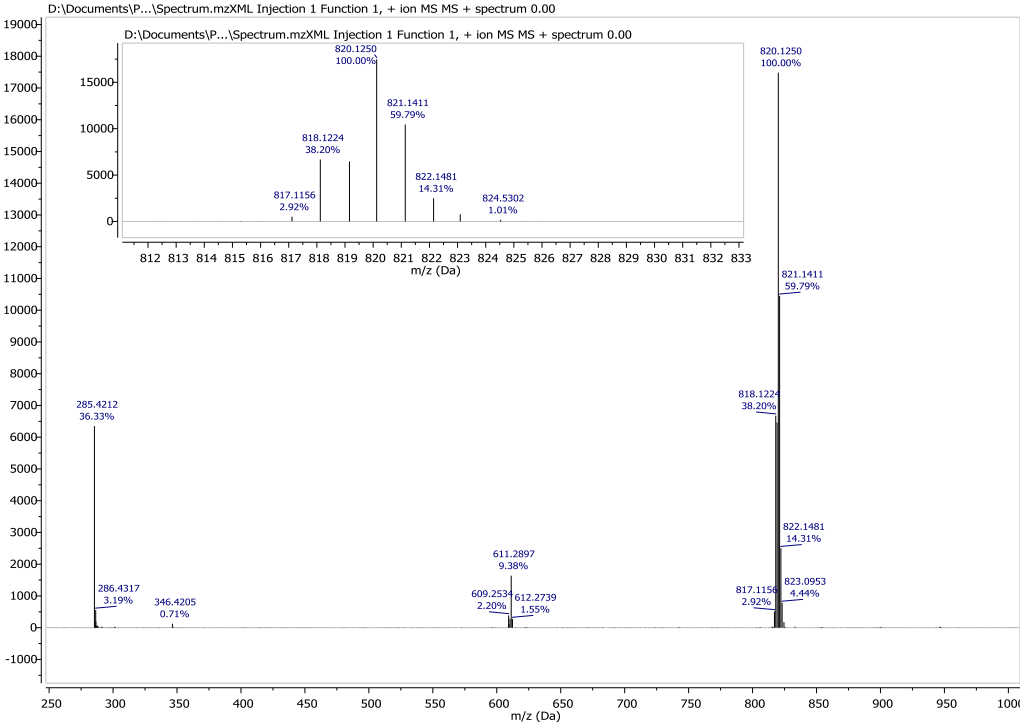

Figure S45. MALDI spectrum of *mer*-Ir(pmpz)$_3$.

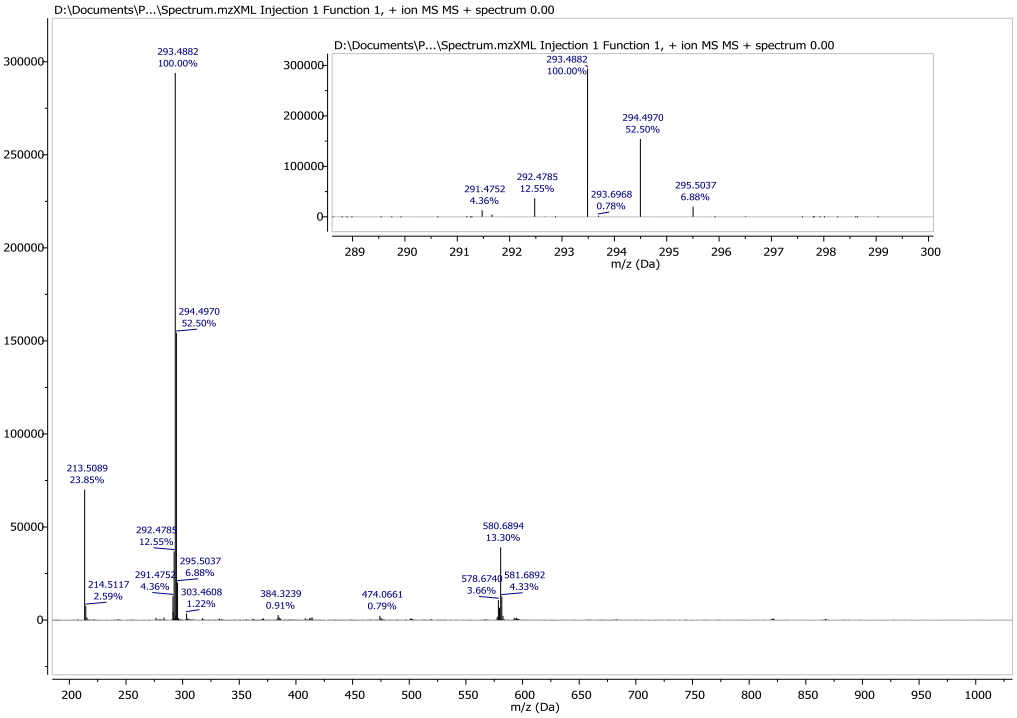

Figure S46. MALDI spectrum of **5**.

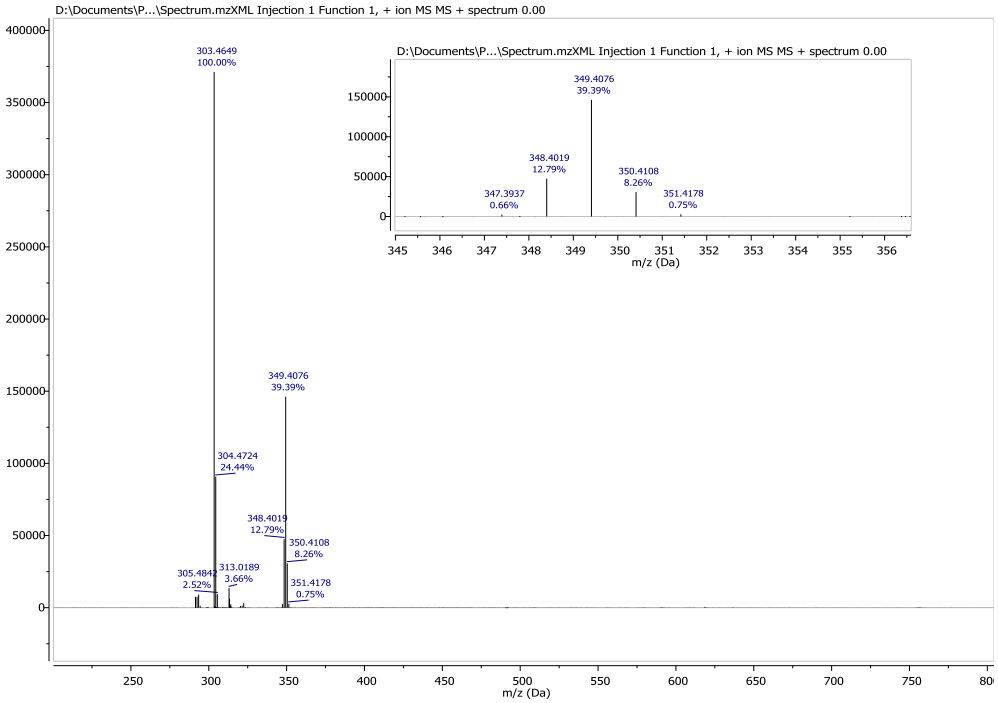

Figure S47. MALDI spectrum of **6**.

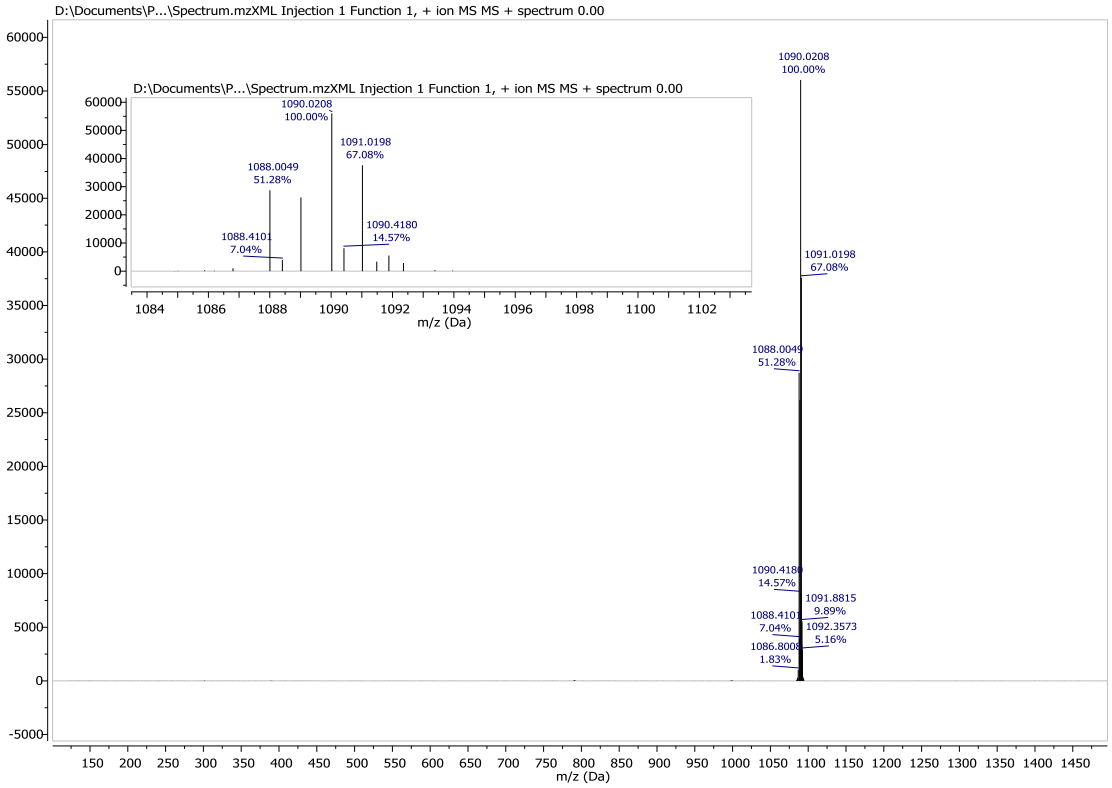

Figure S48. MALDI spectrum of *fac*-Ir(tpz)$_3$.

OLED Fabrication and Characterization:

Glass substrates with pre-patterned, 1 mm wide indium tin oxide (ITO) stripes were cleaned by sequential sonication in tergitol, deionized water, acetone, and isopropanol, followed by 15 min UV ozone exposure. Organic materials and metals were deposited at rates of 0.5-2 Å/s through shadow masks in a vacuum thermal evaporator with a base pressure of 10^{-7} Torr. A separate shadow mask was used to deposit 1 mm wide stripes of 100 nm thick Al films perpendicular to the ITO stripes to form the cathode, resulting in 2 mm^2 device area. The device structure is: glass substrate / 70 nm ITO / 5 nm dipyrazino[2,3,-f:20,30-h]quinoxaline 2,3,6,7,10,11-hexacarbonitrile (HATCN) / 40 nm 4,4′-cyclohexylidenebis [N,N-bis(4-methylphenyl)benzenamine] (TAPC) /8 vol% *fac*-Ir(tpz)$_3$:Host / 45 nm BP4mPy / 1.5 nm 8-hydroxyquinolinato lithium (LiQ) / 100 nm Al. The host is either 3,3'-di(9H-carbazol-9-yl)-1,1'-biphenyl (*m*CBP) or 1-(4-(dibenzo[b,d]thiophen-4-yl)-2,5-dimethylphenyl)-1H-phenanthro[9,10-*d*]imidazole (txI).

A semiconductor parameter analyzer (HP4156A) and a calibrated large area photodiode that collected all light exiting the glass substrate were used to measure the *J*-*V*-luminance characteristics. The device spectra were measured using a fiber-coupled spectrometer.

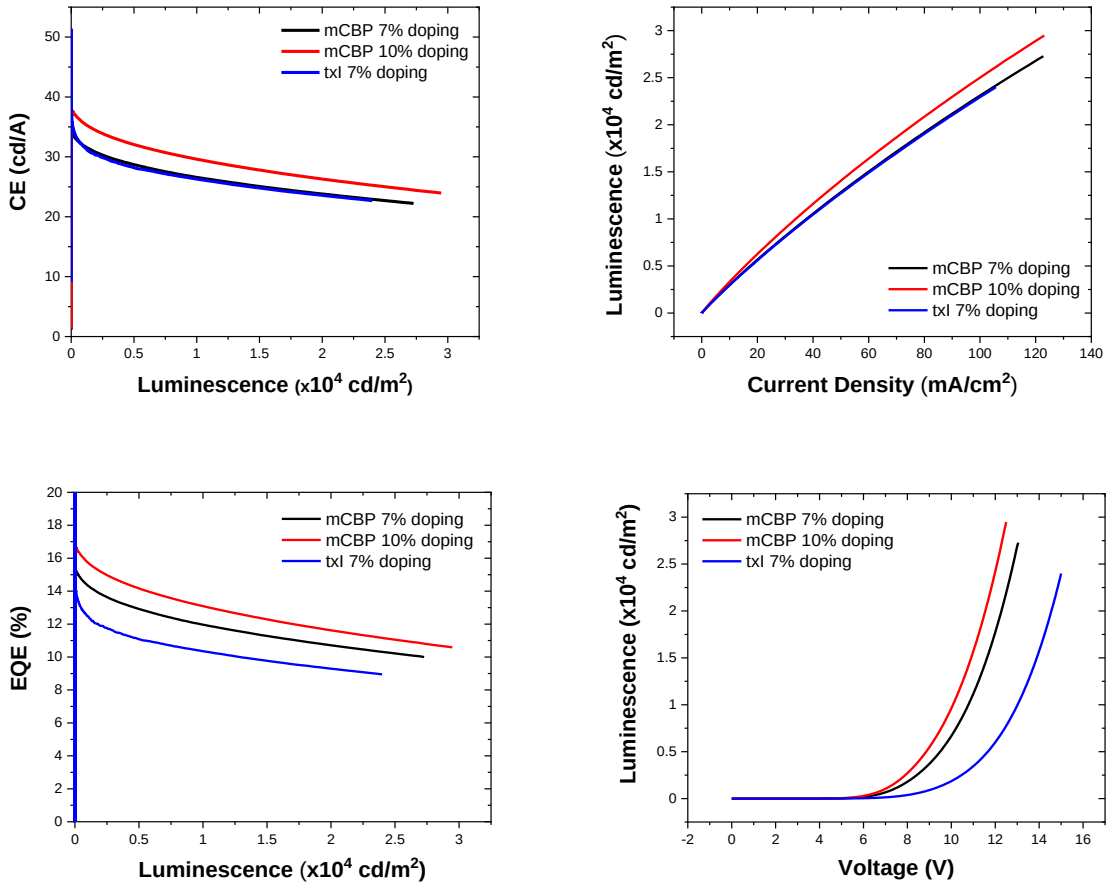

Figure S49. OLED device characteristics using *fac*-Ir(tpz)$_3$ as a dopant.

References

1. A. Freitag, P. Prajwal, A. Shymanets, C. Harteneck, B. Nürnberg, C. Schächtele, M. Kubbutat, F. Totzke and S. A. Laufer, *Journal of Medicinal Chemistry*, 2015, **58**, 212-221.
2. Y. H. Shao, Z. T. Gan, E. Epifanovsky, A. T. B. Gilbert, M. Wormit, J. Kussmann, A. W. Lange, A. Behn, J. Deng, X. T. Feng, D. Ghosh, M. Goldey, P. R. Horn, L. D. Jacobson, I. Kaliman, R. Z. Khaliullin, T. Kus, A. Landau, J. Liu, E. I. Proynov, Y. M. Rhee, R. M. Richard, M. A. Rohrdanz, R. P. Steele, E. J. Sundstrom, H. L. Woodcock, P. M. Zimmerman, D. Zuev, B. Albrecht, E. Alguire, B. Austin, G. J. O. Beran, Y. A. Bernard, E. Berquist, K. Brandhorst, K. B. Bravaya, S. T. Brown, D. Casanova, C. M. Chang, Y. Q. Chen, S. H. Chien, K. D. Closser, D. L. Crittenden, M. Diedenhofen, R. A. DiStasio, H. Do, A. D. Dutoi, R. G. Edgar, S. Fatehi, L. Fusti-Molnar, A. Ghysels, A. Golubeva-Zadorozhnaya, J. Gomes, M. W. D. Hanson-Heine, P. H. P. Harbach, A. W. Hauser, E. G. Hohenstein, Z. C. Holden, T. C. Jagau, H. J. Ji, B. Kaduk, K. Khistyaev, J. Kim, R. A. King, P. Klunzinger, D. Kosenkov, T. Kowalczyk, C. M. Krauter, K. U. Lao, A. D. Laurent, K. V. Lawler, S. V. Levchenko, C. Y. Lin, F. Liu, E. Livshits, R. C. Lochan, A. Luenser, P. Manohar, S. F. Manzer, S. P. Mao, N. Mardirossian, A. V. Marenich, S. A. Maurer, N. J. Mayhall, E. Neuscamman, C. M. Oana, R. Olivares-Amaya, D. P. O'Neill, J. A. Parkhill, T. M. Perrine, R. Peverati, A. Prociuk, D. R. Rehn, E. Rosta, N. J. Russ, S. M. Sharada, S. Sharma, D. W. Small, A. Sodt, T. Stein, D. Stuck, Y. C. Su, A. J. W. Thom, T. Tsuchimochi, V. Vanovschi, L. Vogt, O. Vydrov, T. Wang, M. A. Watson, J. Wenzel, A. White, C. F. Williams, J. Yang, S. Yeganeh, S. R. Yost, Z. Q. You, I. Y. Zhang, X. Zhang, Y. Zhao, B. R. Brooks, G. K. L. Chan, D. M. Chipman, C. J. Cramer, W. A. Goddard, M. S. Gordon, W. J. Hehre, A. Klamt, H. F. Schaefer, M. W. Schmidt, C. D. Sherrill, D. G. Truhlar, A. Warshel, X. Xu, A. Aspuru-Guzik, R. Baer, A. T. Bell, N. A. Besley, J. D. Chai, A. Dreuw, B. D. Dunietz, T. R. Furlani, S. R. Gwaltney, C. P. Hsu, Y. S. Jung, J. Kong, D. S. Lambrecht, W. Z. Liang, C. Ochsenfeld, V. A. Rassolov, L. V. Slipchenko, J. E. Subotnik, T. Van Voorhis, J. M. Herbert, A. I. Krylov, P. M. W. Gill and M. Head-Gordon, *Mol. Phys.*, 2015, **113**, 184-215.
3. G. Hermann, V. Pohl, J. C. Tremblay, B. Paulus, H. C. Hege and A. Schild, *Journal of Computational Chemistry*, 2016, **37**, 1511-1520.
4. S. G. P. Castro, A. Loukianov and e. al., *Journal*, 2020, DOI: 10.5281/zenodo.2541552.